Published in final edited form as:

*Cell Rep*. 2022 June 07; 39(10): 110853. doi:10.1016/j.celrep.2022.110853.

# CPEB3-dependent increase in GluA2 subunits impairs excitatory transmission onto inhibitory interneurons in a mouse model of fragile X

**Jee-Yeon Hwang**[1,6,11,13,*], **Hannah R. Monday**[1,10,11], **Jingqi Yan**[1,5,11], **Andrea Gompers**[1,7,11], **Adina R. Buxbaum**[1,2,3,8], **Kirsty J. Sawicka**[1,9], **Robert H. Singer**[1,2,3,12], **Pablo E. Castillo**[1,4,12], **R. Suzanne Zukin**[1,12,*]

[1]Dominick P. Purpura Department of Neuroscience, Albert Einstein College of Medicine, New York, NY 10461, USA

[2]Department of Structural & Cell Biology, Albert Einstein College of Medicine, New York, NY 10461, USA

[3]Janelia Research Campus, Howard Hughes Medical Institute, Ashburn, VA 20147, USA

[4]Department of Psychiatry and Behavioral Sciences, Albert Einstein College of Medicine, New York, NY 10461, USA

[5]Center for Gene Regulation in Health and Disease, Department of Biological, Geological, and Environmental Sciences, Cleveland State University, Cleveland, OH 44115, USA

[6]Department of Pharmacology and Neuroscience, Creighton University School of Medicine, Omaha, NE 68178, USA

[7]Center for Immunology and Infectious Diseases, University of California, Davis, Davis, CA 95616, USA

[8]Present address: Department of Neurosciences, University of California, San Diego, La Jolla, CA 92093, USA

[9]Present address: Cancer Research UK Cambridge Institute, Li Ka Shing Centre, University of Cambridge, Cambridge, UK

[10]Present address: Department of Molecular and Cellular Biology and Helen Wills Neuroscience Institute, University of California, Berkeley, Berkeley, CA 94720, USA

[11]These authors contributed equally



[*]Correspondence: jeeyeonhwang@creighton.edu (J.-Y.H.), suzanne.zukin@einsteinmed.org (R.S.Z.).

AUTHOR CONTRIBUTIONS

J.-Y.H., H.R.M., J.Y., A.G., A.R.B., R.H.S., P.E.C., and R.S.Z. designed the research. J.-Y.H., H.R.M., J.Y., A.G., A.R.B., and K.J.S. performed the research. J.-Y.H., H.R.M., J.Y., A.G., and A.R.B. analyzed data. J.-Y.H., H.R.M., J.Y., A.G., A.R.B., K.J.S., R.H.S., P.E.C., and R.S.Z. interpreted the data and wrote the paper.

SUPPLEMENTAL INFORMATION

Supplemental information can be found online at https://doi.org/10.1016/j.celrep.2022.110853.

DECLARATION OF INTERESTS

The authors declare no competing interests.

[12]These authors contributed equally

[13]Lead contact

## SUMMARY

Fragile X syndrome (FXS) is a leading cause of inherited intellectual disability and autism. Whereas dysregulated RNA translation in *Fmr1* knockout (KO) mice, a model of FXS, is well studied, little is known about aberrant transcription. Using single-molecule mRNA detection, we show that mRNA encoding the AMPAR subunit GluA2 (but not GluA1) is elevated in dendrites and at transcription sites of hippocampal neurons of *Fmr1* KO mice, indicating elevated GluA2 transcription. We identify CPEB3, a protein implicated in memory consolidation, as an upstream effector critical to GluA2 mRNA expression in FXS. Increased GluA2 mRNA is translated into an increase in GluA2 subunits, a switch in synaptic AMPAR phenotype from GluA2-lacking, $Ca^{2+}$-permeable to GluA2-containing, $Ca^{2+}$-impermeable, reduced inhibitory synaptic transmission, and loss of NMDAR-independent LTP at glutamatergic synapses onto CA1 inhibitory interneurons. These factors could contribute to an excitatory/inhibitory imbalance—a common theme in FXS and other autism spectrum disorders.

## Graphical Abstract

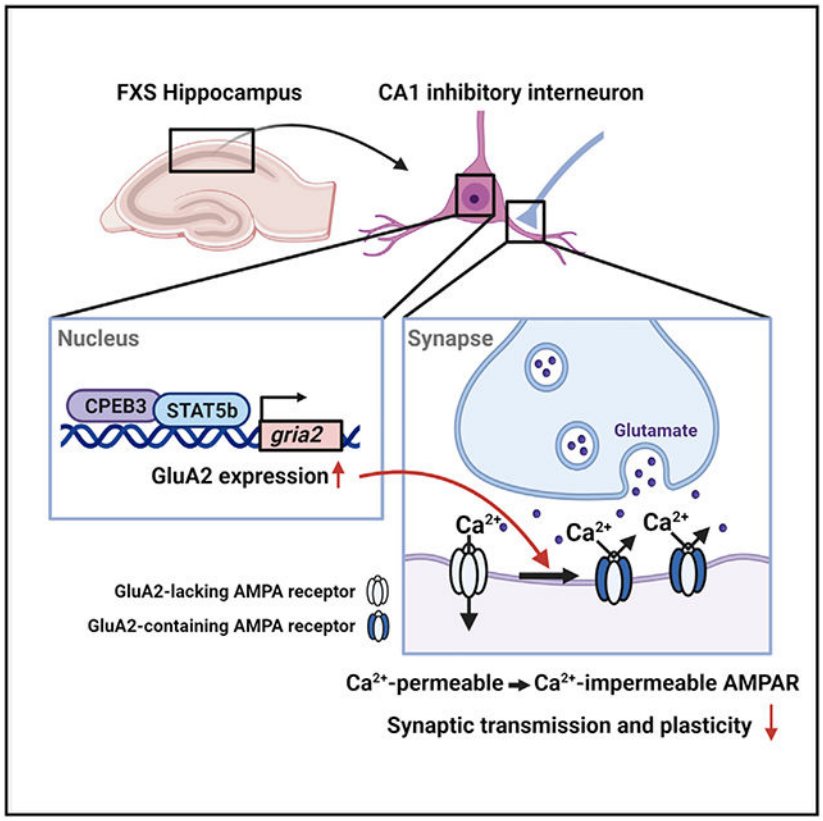


## In brief

Using single-molecule FISH and patch-clamp recording, Hwang et al. show that dysregulation of GluA2 transcription is critical to synaptic function in an animal model of autism. The increase in GluA2 results in a switch in AMPAR phenotype and deficits in synaptic transmission and plasticity at synapses onto CA1 inhibitory interneurons.

## INTRODUCTION

Fragile X syndrome (FXS) is the most common inherited form of intellectual disability and autism (Bagni and Zukin, 2019; Bhakar et al., 2012; Darnell and Klann, 2013; Richter et al., 2015) and is caused by the expansion of a CGG repeat sequence in the 5′ untranslated region (UTR) of the *FMR1* gene, resulting in silencing and loss of its gene product fragile X mental retardation protein (FMRP), an RNA binding protein (Fu et al., 1991; Pieretti et al., 1991). Patients with FXS exhibit mild to severe cognitive impairment, a decrease in the threshold for seizures, emotional instability, heightened sensitivity to sensory stimulus, sleep disorders, attentional deficits, and autism (Hagerman and Hagerman, 2013; Hagerman et al., 2017; Ronesi and Huber, 2008). FXS and other autism spectrum disorders (ASDs) are characterized by a heightened excitation/inhibition (E/I) imbalance throughout the brain, which is thought to underlie some symptoms associated with FXS (Antoine et al., 2019; Nelson and Valakh, 2015). FMRP plays a critical role in the translational repression of >1,000 putative target mRNAs, many of which encode synaptic proteins (Ascano et al., 2012; Darnell et al., 2011) (but see Sawicka et al., 2019). Whereas elevated protein translation (Darnell and Klann, 2013) and impaired protein degradation (Hwang et al., 2019; Yan et al., 2018) are well established in neurons of *Fmr1* knockout (KO) mice, little is known about dysregulation of transcription.

AMPA receptors (AMPARs) mediate fast excitatory transmission and are comprised of four subunits, GluA1–4. The AMPAR GluA2 subunit governs AMPAR $Ca^{2+}$ permeability and rectification properties, thereby determining the phenotype of synaptic AMPARs (Liu and Zukin, 2007). The GluA2 subunit also influences channel kinetics, conductance, AMPAR assembly, forward trafficking from the endoplasmic reticulum, and targeting to and from synaptic sites (Isaac et al., 2007; Liu and Zukin, 2007). Importantly, in the mature brain, principal neurons of the hippocampus are thought to express GluA2-containing, $Ca^{2+}$-impermeable AMPARs (Lu et al., 2009), whereas inhibitory interneurons express primarily GluA2- lacking, $Ca^{2+}$-permeable AMPARs (Akgul and McBain, 2016), as assessed by single-cell genetic analysis in the intact mouse and electrophysiology in hippocampal slices (Akgul and McBain, 2016; Lu et al., 2009). This functional difference is supported by previous evidence that pyramidal cells and other principal neurons of the hippocampus contain almost exclusively GluA1 and GluA2 mRNA, whereas most neighboring inhibitory interneurons contain almost exclusively GluA1 mRNA and, to a lower extent, GluA2 and 3 (Geiger et al., 1995; Racca et al., 1996). Thus, a switch in AMPAR phenotype from GluA2-lacking to GluA2-containing at synapses onto inhibitory interneurons would likely require transcription of new GluA2 mRNA. Inhibitory interneurons express an NMDA receptor (NMDAR)-independent form of synaptic plasticity that relies on $Ca^{2+}$ influx through AMPAR receptors (Kullmann and Lamsa, 2007). Thus, even a modest increase

in GluA2 mRNA would have an important impact on synaptic efficacy and plasticity at synapses onto these neurons.

This study was undertaken to examine mechanisms underlying GluA1 and GluA2 mRNA targeting to dendrites and transcription and their impact on synaptic plasticity in *Fmr1* null versus wild-type (WT) neurons. Using single-molecule fluorescence *in situ* hybridization (FISH) to detect individual AMPAR mRNA molecules (Femino et al., 1998; Raj et al., 2008), we show that mRNA encoding the AMPAR subunit GluA2 (but not that encoding GluA1) is elevated in proximal dendrites and at transcription sites in *Fmr1* KO neurons. Because FMRP does not bind or regulate mRNAs encoding GluA2 directly in hippocampal neurons (Darnell et al., 2011; Sawicka et al., 2019), we focused on upstream effectors that might regulate GluA2 mRNA targeting or transcription. We identify cytoplasmic element binding protein 3 (CPEB3), a known FMRP target (Ascano et al., 2012; Sawicka et al., 2019), as an upstream effector critical to dysregulation of GluA2 mRNA expression and targeting to dendrites in *Fmr1* KO mice. This is significant in that CPEB3 is implicated in synaptogenesis, synaptic plasticity, and hippocampal-based memory (Fioriti et al., 2015; Pavlopoulos et al., 2011). We identify a mechanism by which CPEB3 increases GluA2 transcription. CPEB3 localizes with STAT5b at the *gria2* promoter, where it promotes active transcription of GluA2 through its interaction with STAT5b, an effect augmented in *Fmr1*-deficient neurons. Using immunofluorescence and whole-cell recording from acute hippocampal slices, we show that the increase in GluA2 transcription is translated into an increase in GluA2 protein, a switch in synaptic phenotype, and loss of NMDAR-independent LTP at glutamatergic synapses onto inhibitory interneurons in CA1, findings that may have strong implications for the impaired E/I balance and cognition observed in FXS.

## RESULTS

### mRNAs encoding AMPAR subunits are present in dendrites and at synaptic sites

Because FMRP, the gene product of the *Fmr1* gene, is an RNA binding protein that regulates the localization and translation of a large number of target mRNAs and AMPARs mediate fast synaptic transmission and are critical to most forms of synaptic plasticity, we focused on mRNAs encoding the AMPAR subunits GluA1 and GluA2. We examined the precise spatial distribution of AMPAR mRNAs within somatodendritic compartments of the neuron by single-molecule FISH and immunofluorescence for the dendritic marker MAP2 and the presynaptic marker bassoon in hippocampal neurons from WT mice. GluA1 (Figure 1A) and GluA2 (Figure 1B) mRNA molecules were clearly visible in MAP2-labeled dendrites (merge, Figures 1A and 1B). AMPAR RNA molecules localized to dendritic shafts, corroborating our earlier work (Grooms et al., 2006). A subset of GluA1 and GluA2 AMPAR mRNA puncta were juxtaposed to synaptic sites marked by bassoon (Figures 1A and 1B, arrows). Thus, GluA1 and GluA2 mRNA are present in dendrites and apparent synaptic sites, consistent with the possibility of local translation of AMPARs at synaptic sites. GluA1 and GluA2 mRNA molecules imaged in the same dendrite were present at similar levels (Figures 1C–1E), but exhibited little to no colocalization (Figure 1D), consistent with the possibility that the two mRNAs are transported separately as has been shown for mRNAs encoding β-actin, MAP2, and CAMKIIα (Batish et al., 2012; Mikl et al.,

2011). GluA1 and GluA2 mRNA molecules were relatively abundant in proximal dendrites, defined as the first 30 μm from the cell body, but declined sharply with distance from the cell body (Figure 1F), as reported previously (Ho et al., 2014).

Dendritic mRNAs can be packaged in translationally quiescent ribonucleoprotein granules, which may impair the ability of exogenous probes to hybridize with endogenous mRNAs (Buxbaum et al., 2014). To detect all mRNAs encoding AMPARs, neurons were treated with a protease cocktail, which was previously shown to unmask β-actin mRNA contained in granules (Buxbaum et al., 2014). Protease treatment (unmasking) did not detectably alter the number of AMPAR mRNAs visualized in dendrites of WT neurons (data not illustrated), indicating that the relatively small number of endogenous AMPAR mRNA molecules visualized in WT dendrites is not due to masking of mRNAs by RNA binding proteins.

## GluA2 (but not GluA1) mRNA is elevated in dendrites and at transcription sites of *Fmr1*-deficient neurons

Because FMRP is an RNA binding protein and its absence could result in unchecked translation of target mRNAs, we next examined individual GluA1 (Figures 2A–2D) and GluA2 (Figures 2E–2H) mRNAs in dendrites of hippocampal neurons from *Fmr1* KO and WT mice by single-molecule detection. We focused on GluA1 and GluA2 because these are the subunits that assemble to form nearly all AMPARs in the mature hippocampus (Lu et al., 2009). Whereas the number of endogenous GluA1 mRNA molecules did not detectably differ in dendrites of hippocampal neurons from the two genotypes (Figures 2C and 2D), the number of GluA2 mRNA molecules was markedly greater in the dendrites of *Fmr1* KO versus WT neurons (Figures 2G and 2H). The finding that the number of GluA2, but not GluA1, mRNA molecules is elevated in the proximal region of *Fmr1* KO dendrites is consistent with a model whereby the two mRNAs are differentially regulated and transported and that GluA2 mRNA expression, transport, and/or stability differs in *Fmr1* KO versus WT neurons.

A possible mechanism by which GluA2 mRNA might be altered in *Fmr1* KO neurons is that of enhanced transcription. Single-molecule FISH provides an absolute quantification of mRNA transcription at sites within the nucleus of hippocampal neurons, affording an approximate quantification of mRNA synthesis rates (Larson et al., 2009; Zenklusen et al., 2008). To examine single GluA2 mRNA molecules at transition sites (TSSs), we performed single-molecule FISH with probes directed to coding and intronic sequences within the *gria2* gene. In WT neurons, we observed one to two large, bright spots in essentially all nuclei of all neurons within the field of view, consistent with the notion that AMPAR mRNAs are synthesized continuously (Figure 2I). To confirm that the bright puncta observed in the nucleus are indeed sites of active transcription, we performed dual FISH labeling with probes that target coding (Figure 2I, upper left) and intronic (Figure 2I, upper right) sequences within the *gria2* gene (Figure 2I, lower left). Whereas coding probes label nascent and mature RNAs, intronic probes label only genomic DNA or pre-mRNA (“nascent RNA”), but not mature mRNA. We observed colocalization of GluA2 mRNA encoding AMPAR subunits together with genomic DNA (Figure 2I, upper left and right, indicated by arrows in

panels) in nuclei marked by DAPI, confirming their localization at TSSs (Figure 2I, lower right). To determine whether mature GluA1 and GluA2 mRNAs are present at TSSs and whether the number of nascent mRNA molecules differs in *Fmr1* KO versus WT neurons, we quantified the number of mRNAs at TSSs of *Fmr1* KO and WT neurons. Whereas the number of individual nascent GluA1 mRNA molecules at TSSs did not detectably differ in *Fmr1* KO versus WT neurons (Figures 2J and 2K, upper), the number of nascent GluA2 mRNA molecules at TSSs was markedly greater in *Fmr1* KO versus WT neurons (Figures 2J and 2K, lower), indicative of enhanced GluA2 (but not GluA1) mRNA transcription rate in *Fmr1* KO neurons. To verify that these results also apply to intact tissue, we performed qRT-PCR for GluA1 and GluA2 on lysates of whole hippocampus (Figure 2l). Whereas GluA1 mRNA expression did not differ detectably between the two genotypes, GluA2 mRNA expression was higher in *Fmr1* KO mice.

## CPEB3 protein is elevated in dendrites and TSSs and is critical to elevated GluA2 mRNA

The findings thus far show that the number of GluA2 mRNA molecules is elevated in dendrites and at TSSs of hippocampal neurons from *Fmr1* KO versus WT mice, but do not address the mechanism underlying this increase. Because FMRP does not bind GluA2 mRNA directly or regulate its translation in mouse brain (Darnell et al., 2011), we reasoned that FMRP might regulate an upstream effector of GluA2 mRNA. The sequence-specific RNA binding protein CPEB3 binds a recognition motif harbored within the 3′ UTR of GluA2 (but not GluA1) mRNA, thereby regulating GluA2 (but not GluA1) mRNA transport and polyadenylation-induced translation (Huang et al., 2006) and is a known target of FMRP (Ascano et al., 2012; Sawicka et al., 2019). To determine whether the increase in GluA2 mRNA observed in dendrites of *Fmr1* KO neurons coincides with an increase in CPEB3 protein in dendrites, we performed immunolabeling with an antibody directed to CPEB3 in primary cultures of hippocampal neurons from WT and *Fmr1* KO mice (Figure 3A). Whereas GluA2 mRNA was elevated in the nucleus and proximal dendrites of *Fmr1* KO versus WT neurons (Figures 2G and 2H), CPEB3 abundance was elevated throughout the neuron, including the nucleus (Figures 3A–3C), consistent with its known nuclear localization sequence and dendrites, consistent with a role in targeting GluA2 mRNA.

To address a possible causal relation between elevated CPEB3 protein and elevated GluA2 mRNA, we designed two shRNA constructs that target different sequences within CPEB3 and a nontargeting (NT) shRNA that does not target any known vertebrate sequence (negative control; Figure 3D). To validate the specificity of shRNAs to CPEB3, we transduced hippocampal neurons with a self-inactivating lentivirus carrying either of the two shRNAs directed to CPEB3 or NT shRNA (Figure 3D). Whereas shRNA-1 to CPEB3 (shCPEB3–1) and shCPEB3–2 (not illustrated), but not NT shRNA, knocked down CPEB3, they had little or no effect on the structurally related protein CPEB1, assessed by western blots (Figure 3E). These findings validate the efficacy and specificity of the shRNA constructs.

We reasoned that if elevated levels of CPEB3 increased GluA2 mRNA in *Fmr1* KO neurons, then shRNA-mediated knockdown of CPEB3 would be expected to rescue the number of mRNAs encoding the AMPAR subunit GluA2 in dendrites of *Fmr1* KO neurons. Toward

this end, we labeled GluA2 mRNA in hippocampal neurons from WT (Figure 3F) and *Fmr1* KO (Figure 3G) mice expressing shCPEB3–1 or NT shRNA (negative control) by means of single-molecule FISH. shCPEB3, but not NT shRNA, restored the number of GluA2 mRNA molecules in dendrites of *Fmr1* KO neurons to levels near that observed in WT neurons (Figure 3H). These findings indicate that CPEB3 protein abundance is elevated and critical to the elevated number of GluA2 mRNA molecules in dendrites of *Fmr1* KO versus WT neurons.

We next examined the relation between elevated CPEB3 protein and elevated nascent GluA2 mRNA at TSSs of WT and *Fmr1* KO neurons. We performed genetic manipulation of CPEB3, followed by quantitative single-molecule FISH to detect GluA1 or GluA2 mRNA. Acute knockdown of CPEB3 in *Fmr1* KO neurons with shCPEB3, but not NT shRNA (Figures 3I and 3J), restored the number of GluA2 mRNA molecules at TSSs to near that observed in WT neurons (Figure 3K). In contrast, CPEB3 knockdown did not significantly alter the number of GluA1 mRNA molecules at TSSs (Figure S1), indicating specificity of the CPEB3 shRNA for its target mRNA. Overexpression of GFP-tagged CPEB3, but not GFP alone (Figures 3L and 3M), markedly increased the number of GluA2 mRNA molecules at TSSs and in the nucleus of WT hippocampal neurons to near that observed in *Fmr1* KO neurons (Figure 3N). These data reveal a causal relationship between CPEB3 protein and the number of GluA2 mRNA molecules in hippocampal neurons and suggest a mechanism by which GluA2 mRNA levels are regulated in *Fmr1* KO mice. Finally, we examined CPEB3 protein expression in brain sections at the level of the hippocampus by immunofluorescence. CPEB3 immunofluorescence was robust in cell bodies and dendrites of CA1 neurons marked by NeuN in brain sections from WT and *Fmr1* KO mice (Figure 3O). Quantification of immunofluorescence data indicated that CPEB3 was ~2.5-fold higher in the CA1 of *Fmr1* KO versus WT mice (Figure 3P).

## Loss of FMRP is causally related to the elevated CPEB3 in fragile X neurons

Elevated CPEB3 abundance in dendrites of *Fmr1* KO mice could arise as a consequence of altered CPEB3 transcription or post-transcriptional mechanisms. To distinguish between these mechanisms, we performed qRT-PCR on lysates of hippocampal neurons from WT and *Fmr1* KO mice. CPEB3 mRNA abundance was not detectably different in hippocampal neurons from *Fmr1* KO versus WT mice (Figure 4A), suggesting that the increase in CPEB3 is unlikely to occur via altered transcription or mRNA stability. By contrast, CPEB3 protein abundance was elevated (by ~7-fold) in hippocampal neurons from *Fmr1* KO versus WT mice, as assessed by western blot analysis (Figure 4B). Consistent with this, shRNA-induced knockdown of FMRP in WT neurons markedly increased CPEB3 protein abundance to near that observed in neurons from *Fmr1* KO mice (Figure 4C). To determine whether loss of FMRP is causally related to elevated CPEB3 protein in *Fmr1* KO neurons, we expressed human FMRP (hFMRP) in *Fmr1* KO neurons and examined the impact of reintroduction of FMRP on CPEB3 protein expression. Overexpression of hFMRP in *Fmr1* KO neurons restored elevated levels of CPEB3 protein to near those of WT neurons (Figure 4D). These findings suggest that FMRP regulates CPEB3 protein abundance either directly or indirectly at the level of protein synthesis and/or stability, consistent with the role of FMRP as a translational repressor.

### CPEB3 and STAT5b are enriched at the *gria2* promoter

The results thus far show that CPEB3 drives the increase in GluA2 mRNA in hippocampal neurons, but does not address mechanism. To address this issue, we next assessed the mechanism by which CPEB3 might increase GluA2 mRNA transcription rate. To identify consensus binding motifs for transcription factors within the promoter region of *gria2* (gene encoding GluA2), we used Jaspar software set at high stringency. We identified an exact match to the known recognition motif for the transcription factor STAT5b contained within the TSS of the *gria2* proximal promoter (Figure 5A). To determine whether STAT5b binds the putative STAT5b recognition site within the *gria2* promoter and promotes active transcription of GluA2, we performed chromatin immunoprecipitation (ChIP) on hippocampal tissue from WT and *Fmr1* KO mice. In the hippocampus of WT mice, STAT5b binding was enriched and spatially restricted to the putative Stat5b recognition motif within the proximal promoter of *gria2*; in contrast, STAT5b did not bind at other sites proximal (150 or 350 bp upstream) or distal (at 2 kb upstream or 10 kb downstream) to the TSS of the *gria2* promoter, indicating specificity of STAT5b binding to the *gria2* promoter (Figure 5B). In hippocampal tissue from *Fmr1* KO mice, binding of STAT5b to the predicted STAT5b binding site within the TSS of the *gria2* promoter and at two sites proximal (150 and 350 bp upstream), but not at sites distal (2or 10 kb downstream) to the TSS of the *gria2* promoter, was intensified relative to that in the hippocampus of WT mice (Figure 5B).

We reasoned that if CPEB3 regulates GluA2 transcription, CPEB3 would likely be enriched at the *gria2* promoter. In samples of hippocampal tissue from WT mice, CPEB3 co-localized with STAT5b at the TSS of the *gria2* promoter (Figure 5A). In hippocampal tissue from *Fmr1* KO mice, CPEB3 enrichment was increased at sites occupied by STAT5b, the STAT5b binding site, and sites proximal (150 and 350 bp upstream), but not distal (2 kb upstream or 10 kb downstream) to the TSS, consistent with enhanced CPEB3 expression in *Fmr1* KO neurons (Figure 5C).

The results thus far show that the transcriptional activator STAT5b and the memory protein CPEB3 are enriched at the *gria2* promoter and that the degree of enrichment of each factor is greater in the hippocampus of *Fmr1* KO versus WT mice, but do not address a causal relation between recruitment of CPEB3 and STAT5b to the *gria2* promoter. Toward this end, we took two approaches. First, we transduced primary cultures of cortical neurons with lentivirus carrying CPEB3 shRNA or NT shRNA and examined STAT5b binding to the proximal promoter of the *gria2* gene (Figure 5D). shCPEB3 (but not NT shRNA) markedly reduced CPEB3 and binding of STAT5b to the putative STAT5b binding motif and at an additional site proximal (150 bp upstream) to the STAT5b binding site within the *gria2* proximal promoter (Figure 5E). In contrast, knockdown of CPEB3 did not detectably alter enrichment of STAT5b at sites distal (750 or 1,000 bp upstream) from the STAT5b binding site in the *gria2* promoter. Second, we delivered NT shRNA into the left hippocampus and CPEB3 shRNA into the right hippocampus in *Fmr1* KO and WT mice. Ten days later, hippocampi were isolated and subjected to ChIP-qPCR. CPEB3 shRNA, but not NT shRNA, markedly reduced binding of STAT5b to the putative STAT5b binding site of the *gria2* promoter and to additional sites in the proximal promoter of the *gria2* promoter (150 and 350 bp upstream), but not at sites distal (2 kb downstream or 10 kb upstream) from the

STAT5b binding site in WT and *Fmr1* KO mice *in vivo* (Figure 5F). These findings, together with data in Figure 3, demonstrate that CPEB3 facilitates STAT5B binding to the *gria2* promoter, and thereby promotes GluA2 transcription. These data reveal a mechanism by which elevated CPEB3 and STAT5b at the *gria2* promoter drive GluA2 transcription and by which GluA2 transcription is increased in hippocampal neurons.

### CA1 inhibitory interneurons of *Fmr1* KO mice express elevated GluA2 protein

We next examined whether elevated GluA2 mRNA in neurons lacking FMRP is translated into increased GluA2 protein. Whereas CA1 pyramidal neurons mainly (if not exclusively) express GluA2-containing AMPARs (Lu et al., 2009), inhibitory interneurons mainly express GluA2-lacking AMPARs (Isaac et al., 2007; Liu et al., 2007). Therefore, excess GluA2 protein in interneurons might convert GluA2-lacking to GluA2-containing AMPARs.

To directly compare changes in mRNA expression with changes in protein, we first performed experiments with primary cultures of hippocampal neurons at days *in vitro* (DIV) 14–17. GluA2 protein abundance was elevated in lysates from hippocampal neurons from *Fmr1* KO versus WT mice, as assessed by western blot analysis (Figure S2A). GluA2 immunolabeling was present throughout cell bodies and dendrites and at synaptic sites (Figure S2B). Quantification of puncta indicated that GluA2 was ~2.2-fold greater at synaptic sites (marked by synapsin) of neurons from *Fmr1* KO versus WT mice (Figure S2C). We next examined GluA2 expression in excitatory versus inhibitory neurons. Toward this end, we labeled neurons with antibodies to vGLUT, a marker for excitatory neurons, or GAD67, a marker for GABAergic inhibitory neurons. Whereas vGLUT(+) excitatory neurons make up ~80% of hippocampal neurons at DIV 14 (Figure S2D), GAD67(+) inhibitory neurons make up ~14% of hippocampal neurons at DIV 14 (Figures S2E). GluA2 was expressed robustly by vGLUT(+) (excitatory) neurons from WT and *Fmr1* KO mice (Figure S2F). Quantification of puncta indicated that GluA2 was elevated modestly (~1.3-fold) in dendrites of vGLUT(+) excitatory neurons from *Fmr1* KO versus WT mice (Figures S2G). In contrast, GluA2 protein expression was modest in GAD(+) inhibitory neurons from WT mice, but was greater in GAD(+) inhibitory neurons from *Fmr1* KO mice (Figure S2H). Quantification of puncta indicated that GluA2 was markedly elevated (~3.4-fold) in dendrites of GAD(+) inhibitory neurons from *Fmr1* KO versus WT mice (Figure S2I). GluA1 protein did not differ detectably in any compartment of hippocampal neurons between the two genotypes (Figure S3).

To determine whether deletion of FMRP also changes AMPAR subunit composition in brain tissue, we performed experiments with hippocampal tissue. We first examined GluA2 protein abundance in the hippocampus by western blot analysis (Figure 6A). GluA2 protein levels were ~1.5 higher in the hippocampal lysates from *Fmr1* KO versus WT mice, as assessed by western blots. We next examined GluA2 protein expression in brain sections in the hippocampus by immunofluorescence. GluA2 immunofluorescence was robust in the cell bodies and dendrites of CA1 neurons in brain sections from *Fmr1* KO versus WT mice (Figure 6B). Quantitation of puncta indicated that GluA2 protein expression was ~1.4 greater in CA1 neurons from *Fmr1* KO versus WT mice (Figure 6C). To examine GluA2 expression in specific cell types within the CA1, we first performed GluA2

immunolabeling of brain sections from *Fmr1* KO and WT mice expressing GFP under the GAD67 promoter (Figure 6D). Colocalization of GluA2 immunofluorescence (red) with GFP-expressing (green) neurons was observed in a small number of neurons scattered in the *stratum pyramidale* and *stratum radiatum* of the CA1 from *Fmr1* KO and WT mice expressing GAD-GFP. Quantification of puncta indicated that GluA2 immunofluorescence in GABAergic GAD67(+)-inhibitory interneurons in the *stratum radiatum* was ~2.4-fold greater in brain sections from *Fmr1* KO versus WT mice (Figure 6E). We next examined GluA2 immunofluorescence (green) in excitatory neurons (marked by CaMKII-mCherry) in the CA1 from *Fmr1* KO and WT mice expressing mCherry under the CAMKII promoter (Figures 6F and 6G). Quantification of puncta indicated that GluA2 immunofluorescence (green) in mCherry(+)-pyramidal neurons was ~1.4-fold greater in brain sections from *Fmr1* KO versus WT mice (Figure 6H). Thus, whereas GluA2 protein is elevated in both inhibitory interneurons and excitatory (pyramidal) neurons in the CA1 of *Fmr1* KO mice, the increase was greater in inhibitory interneurons than in principal neurons.

## AMPA EPSCs at synapses onto interneurons of *Fmr1* KO mice exhibit properties of GluA2-containing AMPARs

Our findings thus far indicate that GluA2 (but not GluA1) protein is elevated in dendrites and at synaptic sites of GABAergic inhibitory interneurons of *Fmr1* KO mice, but do not address synaptic function. Because AMPARs at synapses onto CA1 pyramidal neurons are mainly GluA2 containing (Lu et al., 2009), it is unlikely that an increase in GluA2 expression would significantly alter rectification or other AMPAR properties. On the other hand, at glutamatergic synapses onto inhibitory interneurons, which express mainly GluA2-lacking, $Ca^{2+}$-permeable AMPARs in WT mice, excess GluA2 could result in a switch in AMPAR phenotype. We recorded evoked, AMPAR-mediated excitatory synaptic currents (AMPAR-EPSCs) from inhibitory interneurons in the *stratum radiatum* of CA1 in acute hippocampal slices from WT and *Fmr1* KO mice (P14-P21) at different holding potentials in the presence of intracellularly loaded spermine (Figure 7A). Inclusion of spermine in the pipette solution confers voltage-dependent block of GluA2-lacking AMPARs and a characteristic inwardly rectifying I-V relationship (Bowie and Mayer, 1995; Kamboj et al., 1995). We focused on visually identified CA1 interneurons because our immunofluorescence data indicated evidence of increased GluA2 content in these neurons. The I-V relation of AMPAR-EPSCs recorded from WT inhibitory interneurons showed the expected inward rectification, indicative of GluA2-lacking, $Ca^{2+}$-permeable AMPARs (Le Roux et al., 2013) (Figure 7B, black squares). In contrast, in *Fmr1* KO mice, rectification of AMPAR-EPSCs was decreased (Figure 7B, red squares) and the rectification index was markedly increased at glutamatergic synapses onto inhibitory interneurons (Figure 7C), indicative of an increase in synaptic incorporation of functional GluA2-containing AMPARs (Isaac et al., 2007; Liu and Zukin, 2007). Thus, CA1 interneurons from *Fmr1* KO mice exhibit the electrophysiological signature of an increase in GluA2-containing AMPARs.

## *Fmr1* KO mice exhibit deficits in basal synaptic transmission and LTP at synapses onto interneurons

To examine the consequences of increased GluA2 content on synaptic transmission and plasticity, we recorded EPSC peak amplitudes from visually identified interneurons at five

stimulation intensities from slices of *Fmr1* KO and WT mice. The input-output curve was markedly reduced in slices of *Fmr1* KO mice, relative to that of WT mice (Figure 7D), consistent with an increase in synaptic incorporation of low-conductance GluA2-containing AMPARs and a decrease in high-conductance GluA2-lacking AMPARs (Isaac et al., 2007; Liu and Zukin, 2007). We also tested a form of synaptic plasticity termed NMDAR-independent (or "anti-Hebbian") long-term potentiation (LTP) at glutamatergic synapses onto inhibitory GABAergic interneurons using a protocol in which we paired low-frequency presynaptic activity (400 pulses at 5 Hz) with postsynaptic hyperpolarization to −90 mV in whole-cell configuration (Lamsa et al., 2007). This form of LTP relies on $Ca^{2+}$ influx through GluA2-lacking, $Ca^{2+}$-permeable AMPARs (Kullmann and Lamsa, 2008; Lamsa et al., 2007; Le Roux et al., 2013; Szabo et al., 2012). LTP, defined as at least 25% increase from baseline, at glutamatergic synapses onto inhibitory interneurons was present in six out of the ten cells recorded from slices of WT mice (from six mice) (Figure 7E). Not all WT interneurons showed plasticity, as expected given the heterogeneity of interneuron subtypes in CA1. In contrast and consistent with a requirement for $Ca^{2+}$-permeable, GluA2-lacking-AMPARs, this LTP was absent in slices from *Fmr1* KO mice (zero out of ten cells from five mice) (Figure 7E). Thus, the partial switch in AMPAR subunit phenotype at glutamatergic onto inhibitory GABAergic interneuron synapses in *Fmr1* KO mice is translated into functional deficits in transmission and plasticity in the intact hippocampal circuit.

## DISCUSSION

In this study, using single-molecule FISH to visualize individual mRNAs encoding AMPAR subunits GluA1 and GluA2, we demonstrate elevated GluA2, but not GluA1, at TSSs and in dendrites of hippocampal neurons from *Fmr1* KO mice. The number of GluA2 mRNA molecules in dendrites is relatively small and spatially restricted to the proximal region. We further show that CPEB3, a sequence-specific RNA binding protein known to bind and regulate translation of GluA2 (Ford et al., 2019; Huang et al., 2006), is elevated and causally related to the increase in GluA2 (but not GluA1) transcription. These findings are consistent with a model whereby the memory protein CPEB3 promotes targeting of GluA2 (but not GluA1) mRNA to dendrites and increases the rate of GluA2 transcription. We further show that GluA2 protein is elevated primarily in GAD(67+) inhibitory interneurons and in hippocampal slices from *Fmr1* KO mice, AMPAR-EPSCs at glutamatergic synapses onto inhibitory interneurons, exhibit a switch in electrophysiological signature to that of GluA2-containing, $Ca^{2+}$-impermeable-AMPARs in slices from *Fmr1* KO mice, as demonstrated by a marked decrease in inward rectification. Finally, we show that this "switch" in AMPAR phenotype is associated with reduced basal synaptic transmission and loss of NMDAR-independent LTP at excitatory synapses onto CA1 inhibitory interneurons. Thus, elevated transcription of GluA2 (but not GluA1) mRNA is translated into an increase in GluA2 subunit abundance, a switch in AMPAR phenotype from $Ca^{2+}$-permeable- to more $Ca^{2+}$-impermeable-AMPARs, diminished synaptic transmission, and loss of a major form of synaptic plasticity at synapses onto inhibitory interneurons in a key hippocampal circuit in a mouse model of FXS. Here, we provide a mechanism of synaptic dysfunction, which could

potentially underlie an E/I imbalance, a theme common not only to FXS, but a large number of other ASDs.

We find that increased CPEB3, a protein implicated in memory consolidation, is crucial to elevated GluA2 transcription in hippocampal neurons of *Fmr1* KO mice. In fragile X mice, CPEB3 binding to the *gria2* promoter is augmented, compared with WT mice, and drives the increase in STAT5b binding and GluA2 transcription. CPEB3 was recently identified by HITS-CLIP to be a direct target of FMRP in mouse brain (Sawicka et al., 2019). We hypothesize that in neurons of WT mice, CPEB3, is translationally repressed and GluA2 abundance is normal, whereas in *Fmr1* KO neurons, release of the translational block on CPEB3 results in elevated CPEB3, which drives an increase in GluA2 transcription and GluA2 mRNA targeting to dendrites. Thus, we provide a mechanism whereby loss of FMRP regulates GluA2 mRNA abundance via CPEB3. It should be noted that, whereas previous studies have shown a role for CPEB3 during memory formation by increasing translation of GluA1 and GluA2 and the number of dendritic spines (Pavlopoulos et al., 2011), our study provides molecular and electrophysiological evidence for a selective impact on GluA2 versus GluA1 in inhibitory interneurons of *Fmr1* KO mice, a mouse model of FXS. Whereas we (this study) and others (Pavlopoulos et al., 2011) find that CPEB3 promotes expression of the AMPAR subunit GluA2, Liu and colleagues report that CPEB3 represses GluA2 translation and thereby defines a dendritic gradient of increasing GluA2-containing AMPARs from the cell soma of cerebellar stellate cells (Savtchouk et al., 2016).

Activity-dependent mRNA trafficking and local protein synthesis in dendrites are mechanisms fundamental to synaptic plasticity (Holt and Schuman, 2013; Wang et al., 2010); but see (Ho et al., 2014). Local protein synthesis endows a neuron with the ability to spatially and temporally restrict gene expression within confined compartments (Wang et al., 2010). In support of this, a recent study involving deep sequencing of the neuronal neuropil, followed by high-resolution FISH, identifies >2,500 RNAs in the dendrites of hippocampal neurons (the “synaptic transcriptome”), including mRNAs encoding excitatory and inhibitory receptors (Cajigas et al., 2012). Moreover, stimulation of hippocampal neurons *in vitro* promotes dendritic localization of mRNAs encoding GluA1 and GluA2 (Grooms et al., 2006) and local translation of AMPAR subunits in severed dendrites (Ju et al., 2004; Kacharmina et al., 2000). While we found that GluA2 is upregulated in *Fmr1* KO mice, previous reports using bulk transcriptomic and proteomic analysis have turned up conflicting results as to the regulation of GluA1 and GluA2. Some studies have not reported significant differences in *gria2* expression in *Fmr1* KO versus WT mice (Ceolin et al., 2017; Das Sharma et al., 2019; Ding et al., 2020; Donnard et al., 2020; Korb et al., 2017; Sawicka et al., 2019). Of note, one proteomics study that used a very comparable time point in development to our immunostaining found a similar fold change increase in newly synthesized GluA2 as we did (CITE). These studies use a variety of preparations, including cortical neuron culture, whole frontal cortex lysate, and CA1 pyramidal cell-specific mRNA isolation, across different time windows. We therefore suspect that such discrepancies, which are commonplace in the FXS and transcriptomics/proteomics field, are the result of differences in cell-type, developmental stage, and data processing. Findings in this study that GluA2 transcription and targeting to dendrites are augmented in neurons from *Fmr1* KO

mice represent a conceptual advance in that we document that AMPAR transcription and mRNA trafficking are altered in a disease state.

Our histological and electrophysiological data suggest that the increase in GluA2 transcription is translated into an increase in GluA2 protein in dendrites and at synaptic sites, particularly of hippocampal inhibitory interneurons. Decrease in inward rectification of AMPA EPSCs at these synapses is consistent with a greater synaptic incorporation of GluA2-containing AMPARs. Whereas high-conductance GluA2-lacking AMPARs are permeable to $Ca^{2+}$ and exhibit a characteristic inwardly rectifying current-voltage relation, low-conductance GluA2-containing AMPARs are $Ca^{2+}$ impermeable and electrically linear. Our finding that the input/output function is reduced and that NMDAR-independent LTP is abolished at excitatory synapses onto inhibitory interneurons in FXS mice is consistent with the prediction that even a modest alteration in synaptic GluA2 could have profound implications for synaptic plasticity (Liu and Zukin, 2007). NMDAR-independent or “anti-Hebbian” LTP is a unique form of plasticity that occurs at glutamatergic projections onto inhibitory interneurons at synapses that express GluA2-lacking, $Ca^{2+}$ permeable AMPARs (Kullmann and Lamsa, 2008; Lamsa et al., 2007; Le Roux et al., 2013; Nicholson and Kullmann, 2014; Szabo et al., 2012). This plasticity is thought to occur *in vivo* during sharp wave ripples and lead to recruitment of interneurons during theta wave activity associated with exploration, thereby contributing to spatial memory formation (Lamsa et al., 2007). Thus, the loss of anti-Hebbian LTP in *Fmr1* KO mice might lead to impaired spatial memory, a finding which could have profound implications for the intellectual disabilities associated with FXS. In addition, the reduction in input/output and the loss of LTP suggest that the net inhibitory output of *Fmr1* KO interneurons might be reduced, potentially accounting for changes in E/I balance that have been reported in FXS and other ASDs.

In summary, we provide evidence at the single-molecule level that mRNAs encoding the AMPAR subunit GluA2 (but not GluA1) are elevated in proximal dendrites and at TSSs (indicative of an increased rate of GluA2 transcription [Larson et al., 2009; Zenklusen et al., 2008]) of hippocampal neurons from *Fmr1* KO mice. The memory protein CPEB3 is elevated in the nucleus and in dendrites and is causally related to the increase in GluA2 mRNA at TSSs and targeting and/or stabilization of GluA2 mRNA in dendrites—a putative mechanism by which the AMPAR phenotype is regulated at hippocampal synapses of *Fmr1* KO mice. CPEB3 localizes with Stat5b at the *gria2* proximal promoter and drives STAT5b-dependent transcription, an action that is augmented in *Fmr1* KO neurons. Thus, GluA2 (but not GluA1) transcription is altered in FXS, a disorder typically characterized by aberrant translation and intellectual disabilities. Importantly, the increase in GluA2 transcription is associated with an increase in GluA2 protein at synaptic sites and a switch in AMPAR phenotype from GluA2 lacking to GluA2 containing at excitatory synapses onto inhibitory interneurons in the hippocampus. Given the importance of the GluA2 subunit in determining AMPAR unitary conductance, the change in AMPAR phenotype in inhibitory interneurons could potentially alter the inhibitory to excitatory balance, an important theme in ASDs (Bagni and Zukin, 2019). These findings identify a mechanism relevant to the pathophysiology of FXS that may suggest another direction in research into intellectual disabilities.

### Limitations of the study

Our study has attempted to provide evidence for a causal role of CPEB3 in the regulation of GluA2 transcription in fragile X mice. Proving causality in the context of a disorder characterized by changes in many different proteins is challenging. To this end, we have used multiple shRNAs to manipulate CPEB3 levels to restore GluA2 mRNA levels in dendrites and TSSs and Stat5b binding at the *gria2* promoter in *Fmr1* KO neurons. Conversely, we showed that shRNA knockdown of Fmr1 in WT neurons or expression of human FMRP in KO neurons regulates CPEB3 abundance. One major caveat of many studies in the FXS field, including ours, is that people with FXS typically have CGG repeat expansion in the 5′ UTR of the *Fmr1* gene that leads to hypermethylation at 5′ UTR and causes transcriptional silencing of the *Fmr1* gene, whereas in the mouse model the gene is knocked out. We have utilized multiple models of fragile X, including cultured neurons and acute slices from *Fmr1* KO mice. That our findings remain consistent across models is meant to provide additional support for our model, wherein aberrant CPEB3-mediated regulation of GluA2 transcription leads to changes in basal function and plasticity of excitatory synapses onto inhibitory interneurons in the hippocampus. While such changes in synaptic transmission and plasticity would be expected to alter E/I balance in the hippocampal network, this has not been directly tested, and deserves follow-up.

## STAR★METHODS

### RESOURCE AVAILABILITY

**Lead contact—**Further information and requests for resources and reagents should be directed to and will be fulfilled by the lead contact, Jee-Yeon Hwang (jeeyeonhwang@creighton.edu).

#### Materials availability

- Plasmids generated in this study are available from the lead contact without restriction or with a Materials Transfer Agreement; however, availability of lentiviral particles is limited.
- This study did not generate new unique reagents or mouse lines.

#### Data and code availability

- All data reported in this paper will be shared by the lead contact upon request.
- This paper does not report original code.
- Any additional information required to reanalyze the data reported in this paper is available from the lead contact upon request.

### EXPERIMENTAL MODEL AND SUBJECT DETAILS

**Animals—***Fmr1* KO mice were obtained from the Jackson laboratory. We crossed FVB.129P2-Pde6b + Tyrc-ch *Fmr1*tm1Cgr/J heterozygote females with WT FVB.129P2-Pde6b + Tyrc-ch/AntJ males to obtain littermate progeny of either genotype. GAD-GFP (CB6-Tg(Gad1-EGFP)G42Zjh/J) mice were purchased from the Jackson laboratory. The

breeding cages were maintained in a temperature and light-controlled environment with a 14/10 h light/dark cycle and were treated in accordance with the principles and procedures of the National Institutes of Health *Guide for the Care and Use of Laboratory Animals*. Protocols were approved by the Institutional Animal Care and Use Committee of the Albert Einstein College of Medicine.

**Hippocampal neuronal cell culture—**Primary dissociated cultures of hippocampal neurons were prepared from individual *Fmr1* KO and WT littermates at postnatal day 1. Tails were collected at the time of dissection so genotype could be determined. Hippocampi were isolated, digested with trypsin, triturated and plated on 18 mm poly-L-lysine-coated coverslips at relatively low density (50,000 cells per dish), and maintained in Neurobasal-A medium supplemented with Glutamax and B27 medium (Invitrogen) at 37°C and 5% CO2 until 14–17 d *in vitro (DIV)*. Neurons were treated with 2 μM AraC (Sigma) at *DIV* 4, and media replenished weekly.

**Cells—**HEK293T cells were purchased from ATCC (Cat#: CRL-3216) and cultured at 37°C in 5% CO2 incubator using DMEM culturing media (Gibco, 11995-065) containing 10% FBS, 1% penicillin and streptomycin mixture.

## METHOD DETAILS

**Generation of shRNA and cDNA constructs—**CPEB3 shRNA, *Fmr1* shRNA, and nontargeting (NT) shRNA sequences were engineered in the pcDNA™ 6.2-GW/EmGFP shRNA expression vector (Invitrogen): CPEB3 shRNA-1 (5′-AACTTAAGCCAGACGATAAGGGT-3′); CPEB3 shRNA-2 (5′-TAAATGTACTGC GCGTGGA GAC-3′); *Fmr1 shRNA*-1 (5’-AATATTAGCACCATGAGTACC-3’); *Fmr1* shRNA-2 5’-TAAATCTTCTGGCACCTCCAG-3’); and an NT shRNA, a silencer resistant shRNA sequence that does not target any known eukaryotic gene (5′-AAATGTACTGCGCGT GGAGAC-3′). These were subsequently subcloned into the self-inactivating lentiviral vector pRRLsin.cPPT.CMV.eGFP.Wpre. CPEB3 cDNA was cloned from mouse brain cDNA, utilizing primers to target the 3’ and the 5’ of the coding region and the addition of the Bsrg1/EcoRI restriction site and GFP-hFMRP cDNA was a gift from Jennifer Darnell. We then utilized the EcoRI/Bsrg1 restriction site to clone the cDNA into the FCGW lentiviral construct (gift from Guoping Feng), cutting off the eGFP stop codon to generate eGFP-tagged rCPEB3 or hFMRP. The efficacy of shRNA or cDNA overexpression was evaluated by Western blot analysis 3–7 d after transduction of primary cultures of hippocampal neurons at *DIV* 14–17 expressing endogenous CPEB3 and FMRP. pAAV-CaMKIIa-mCherry construct (#114469) and AAV virus were purchased from Addgene.

**Lentiviral production—**For mRNAi-mediated silencing or cDNA overexpression of CPEB3 in neurons we utilized lentiviral transfer constructs containing hFMRP or CPEB3 cDNA, or CPEB3, *Fmr1* or NT shRNA. High-titer vesicular stomatitis virus-pseudotyped lentiviral stocks were produced in HEK293T by performing calcium phosphate transfection to combine our transfer constructs with the pRSV-REV packaging constructs, and the envelope protein construct pMD2.G as described previously (Miyawaki et al., 2009). Viral

titer was determined by N2A cells transduced with serial dilutions of concentrated lentivirus, and GFP fluorescence was evaluated by flow cytometry at 48 h, after concentration by ultracentrifugation.

**Western blotting—**Hippocampal neurons plated in 6 well plates at 14–17 *DIV* were rinsed in ice-cold 1x phospho-buffered saline supplemented with a 1% cocktail of protease and phosphatase inhibitors (Sigma). Cells were scraped in lysis buffer (25 mM Tris HCl pH 7.4, NaCl 150 mM, EDTA 5 mM pH 8.0, EGTA 5 mM pH 8.0,.5% Triton X-100, supplemented with a 1% (v/v) cocktail of protease and phosphatase inhibitors). Lysates were sonicated and centrifuged to remove insoluble material and protein concentration was determined by the Bradford BCA method with a standard curve. 20–25 μg of protein were run on SDS-PAGE Bis Tris gels (4–12%) (Invitrogen) and probed with specified antibodies. Band density values were normalized to β-actin and quantified in ImageJ (U.S. National Institutes of Health).

**Stereotaxic injection of lentiviral constructs into mice—**For *in vivo* ChIP assay, CPEB3 or NT shRNA was delivered by stereotaxic injection into the hippocampus of live mice at P10. Mice were placed in a stereotaxic device and anesthetized with isoflurane. Concentrated viral solution (1.5 μL) was injected into two positions in the left (NT shRNA) and right (CPEB3 shRNA) hippocampus at a flow rate of 0.2 μL/min. The injection sites were defined by the following two coordinates: 1) 2.1 mm posterior to bregma, 1.4 mm lateral to bregma, 1.8 mm ventral from dura; 2) 3.1 mm posterior to bregma, 2.4 mm lateral to bregma, 2.2 mm ventral from dura. The needle was left in place for an additional 3 min and gently withdrawn. To verify region-specific delivery of the virus, we observed GFP fluorescence in brain sections 10 d after injection. The hippocampal CA1 subfields were microdissected at 10 d after injection and used for ChIP assay.

**Chromatin immunoprecipitation—**Chromatin Immunoprecipitation (ChIP) was performed as described (Noh et al., 2012; Rodenas-Ruano et al., 2012). Hippocampi from 2-week-old WT mice were dissected and submerged in 1% formaldehyde (30 min at room temperature) to cross-link proteins to DNA as previously described. To stop the cross-linking reaction.125 M glycine was added, then the samples were lysed and sonicated to break up DNA in 300 bp fragments. Aliquots of chromatin were diluted with chromatin immunoprecipitation (ChIP) dilution buffer (167 mM NaCl, 16.7 mM Tris-HCl, 1.2 mM EDTA, 0.01% SDS, 1.1% Triton X-100) to a final volume of 1 mL, and 80 μL of pre-immunoprecipitated chromatin reaction was put aside. Preclearing of chromatin from hippocampal lysates was achieved by means of Dynabeads M-280 sheep anti-rabbit IgG (Invitrogen), followed by immunoprecipitation with antibody (10 μg of anti-CPEB3). Immuno-complexes were captured with Dynabeads and eluted in 50 mM Tris, 10 mM EDTA, 1% SDS. To rid samples of protein and unmask mRNAs, samples were treated with proteinase K (Qiagen) and RNAse H (Invitrogen). For ChIP experiments, real-time PCR was performed with SYBR green-tagged primers directed to sequences within the *gria2* proximal promoter.

**RNA extraction and qRT-PCR—**Neurons were washed twice with ice-cold phosphate buffered saline (PBS) and scraped in TRIzol (Invitrogen) and RNA was extracted by means of the Purelink micro to midi kit (Invitrogen) or by phenol chloroform isolation. RNA concentration was measured by means of a Nanodrop (NanoDrop Technologies). Aliquots of RNA (1 μg) were reverse-transcribed to cDNA with SuperScript III Reverse Transcriptase (Invitrogen) using olido d(T) primers. Real-time qPCR was performed as described (Noh et al., 2012; Rodenas-Ruano et al., 2012) with TaqMan probes (Applied Biosystems) for CPEB3 (reference number: Mm01204299_m1) and normalized to GAPDH (reference number: Mm99999915_g1). Reactions were performed in triplicate in a StepOnePlus real-time PCR system (Applied Biosystems). The relative change in mRNA expression was determined by the equation: Fold change = $2^{-\Delta Ct}$ ($\Delta Ct$ = Ct target – Ct reference) where Ct refers to cycle number at which the fluorescence signal crosses a threshold (Livak and Schmittgen, 2001). Relative expression ratio in *Fmr1* KO neurons was calculated by normalization to WT type levels.

**Single molecule fluorescent *in situ* hybridization—**Single molecule Fluorescent in situ Hybridization was performed as described (Buxbaum et al., 2014). In brief, neurons were fixed at room temperature in 4% paraformaldehyde in a cytoskeleton preserving solution consisting of in mM: 10 MES, 138 KCl, 3 $MgCl_2$, 2 EGTA, 320 sucrose, at pH 6.1 for 20 min. Coverslips were rinsed briefly three times in 1X PBS with 0.1 M glycine to quench fixative. Coverslips were dehydrated by incubation in 70% ethanol at 4°C for 16–24 h. Coverslips were warmed to room temperature, and then rehydrated with serial dilutions in 1X PBS with 0.1 M glycine. For prehybridization, coverslips were treated 2X with a solution consisting of 50% formamide and 2X SSC (300 mM sodium chloride, 30 mM sodium citrate), for 10 min at 37°C. Hybridization solution per 18 mm coverslip consisted of in μg: 20 probes, 10 sheared salmon sperm DNA (Invitrogen), 10 *Escherichia coli* RNase-free tRNA and 4 acetylated BSA (Ambion) in 35% formamide, 2X SSC. Coverslips were flipped onto a drop of 50 μL hybridization solution on parafilm and incubated overnight at 37°C in a humidified chamber. The following morning, coverslips were transferred to a 12-well dish, and washed 2X with post-hybridization solution consisting of 20% formamide and 2X SSC, for 10 min at 37°C. Post-hybridization solution was replaced with PBS, and coverslips were mounted with Prolong Gold antifade (Invitrogen) together with DAPI for imaging. 20-nucleotide DNA antisense oligo-probes directed to sequences within the GluA1 coding region, the GluA2 coding region, or GluA2 intronic region, with 48 different Quasar 670 (GluA1 coding region and GluA2 intronic region) or Quasar 570 (GluA2 coding region) from Stellaris (www.biosearchtech.com) were used to visualize single GluA2 or GluA1 mRNAs (Sequences in Table S1).

**Immunofluorescence followed by FISH—**Immunolabeling was performed in a cytoskeleton-preserving solution as described (Grooms et al., 2006), with the exception that immunolabeling was performed prior to processing for FISH. In brief, primary cultures of hippocampal neurons were permeabilized with 0.1% Triton in PBS and then blocked with acetylated BSA (Ambion) for immunofluorescence-FISH or, for immunofluorescence alone, incubated overnight at 4°C with antibodies directed to CPEB3, MAP2, Bassoon, or GluA2,

followed by the appropriate secondary antibody in normal goat serum. For FISH, neurons were processed as described above.

**Microscopy—**Neurons were selected under brightfield microscopy based on cell body size, morphology, and overall health, assessed by the lack of nuclear protrusion, blebbing, disintegration or fasciculation of dendrites, and a clear origin of dendrites from the soma. Cells were imaged with an Upright Olympus BX61 widefield microscope equipped with a 60×1.40 NA oil objective and Sensicam QE cooled Black and White CCD camera. 0.3 μm step Z-stack images were acquired with a motorized stage and 1.5–5 s exposures by means of IP Lab 4.0.8 software.

**Dendritic mRNA analysis—**To analyze the number of individual endogenous mRNAs in dendrites, FISH images were maximally projected and stitched together by means of ImageJ (U.S. National Institutes of Health), and single mRNAs were analyzed by means of the custom made ‘Localize’ software written by D.R. Larson (Singer Lab) for IDL (ITT Visual Information Solutions) as described (Buxbaum et al., 2014; Larson et al., 2009; Zenklusen et al., 2008). Single mRNA intensity and location along straightened dendrites were measured as total intensity beneath a two-dimensional Gaussian fit. The distribution of mRNA molecules was quantified by binning the number of mRNAs in specified regions of the soma along dendrites and then plotting them in Prism. The N’s from these experiments are the number of straightened dendrites, one coverslip per group, and at least 3 independent experiments from 3 different litters, performed on 3 different days. Statistical analysis was assessed by means of a student’s two-tailed *t* test.

**mRNA quantification at transcription sites—**To quantify the number of individual AMPAR mRNAs at transcription sites of single neurons in 3D, we utilized FISH-Quant software in the matlab platform (Mathworks) as described (Mueller et al., 2013). To process images for quantification of individual endogenous mRNAs at transcription sites, raw z-stacks of the FISH image were opened, and transcription sites were outlined and saved. Images were filtered by convolving the raw image with a Gaussian kernel, with 5 times the standard deviation that would best fit the theoretical point spread function of the optical setup used. ROIs were automatically generated to identify transcription sites using a search in an area defined by the nuclear mask and an intensity-based threshold. The number of accumulated nascent mRNAs at transcription sites was quantified by dividing the integrated intensity at the transcription site by the mean intensity of individual mRNA molecules. N values represent the number of hippocampal neurons analyzed from at least 3 independent sets of experiments, each from a different litter of mice. Statistical analysis was assessed by means of one-way ANOVA and a post-hoc Student’s two-tailed *t* test.

**Immunocytochemistry and immunohistochemistry—**For immunocytochemistry, primary cultures of hippocampal neurons were fixed with 4% PFA, blocked with serum from the appropriate species, and subjected to reaction with primary antibodies, followed by reaction with Alexa Fluor 488, 555 or 647 conjugated secondary antibodies (Invitrogen). DAPI staining was used to reveal all cells in the section. At least three coverslips per group and multiple areas per slide selected on a random basis were used for counting analysis.

Images were obtained with a Zeiss LSM880 Airyscan Confocal Microscope (averaged four times). All images were processed using the Image J software (NIH). Labeled neurons were chosen randomly for quantification. For results including intensity normalization, intensities were calculated as integrated puncta intensity for the selected neuron and normalized to the area of the cell body. Quantification was performed by normalizing the puncta intensity of each neuron to that of control samples. To ensure the comparability between preparations, we used the same staining procedure and included all corresponding groups from each experiment. Laser settings of the microscope were uniform across all preparations.

Immunohistochemistry was performed on frozen brain sections from 2–3-week-old Fragile X and WT mice as described (Yan et al., 2018). Mice were anesthetized, transcardially perfused with 4% PFA, and brains were removed, post-fixed for 24 h, and infiltrated with sucrose. Brain sections (20 μm-thick) were blocked with serum from the appropriate species, treated with primary antibodies and then reacted with Alexa Fluor 488, 555 or 647 secondary antibodies (Invitrogen). Naive IgG of the appropriate species was used as a negative control. DAPI staining was used to reveal all cells in brain sections. Images were acquired using the Zeiss LSM880 Airyscan Confocal Microscope and processed using the Image J software (NIH).

**Electrophysiology—**Acute hippocampal slices were prepared from 2–3-week-old *Fmr1* KO male mice or WT littermates. The mice were deeply anesthetized with isoflurane and then killed by decapitation. The brain was removed and quickly placed in ice-cold cutting solution containing the following (in mM): 215 sucrose, 20 glucose, 26 $NaHCO_3$, 4 $MgCl_2$, 4 $MgSO_4$, 1.6 $NaH_2PO_4$, 1 $CaCl_2$, and 2.5 KCl. Hippocampi were mounted on an agar block, and transverse slices 400 μm thick were prepared with a VT1200 S microslicer (Leica). Slices were placed, at room temperature in a holding chamber containing 50% cutting solution and 50% artificial CSF (ACSF) recording solution containing the following (in mM): 124 NaCl, 26 $NaHCO_3$, 10 glucose, 2.5 KCl, 1 $NaH_2PO_4$, 2.5 $CaCl_2$, and 1.3 $MgSO_4$ and was bubbled with 95% $O_2$/5% $CO_2$ (pH 7.4 at 25.0 ± 0.1°C). After 30 min, the 1:1 solution was switched to ACSF at room temperature. Slices recovered in ACSF for at least 1 h, and then were transferred to a submersion-type, temperature-controlled recording chamber (TC-344B, Warner Instruments) and perfused with ACSF at 2 mL/min using a peristaltic pump (Dynamax RP-1, Rainin). To induce excitatory postsynaptic currents (EPSCs), a stimulating pipette (monopolar stimulation) was positioned in stratum radiatum. The stimulating pipette was positioned nearby the soma of the patched interneuron within 100 μm to evoke a monosynaptic response. CA1 stratum radiatum interneurons were identified and voltage-clamped using the visualized patch technique with an internal solution containing the following (in mM): 131 cesium gluconate, 8 NaCl, 1 CaCl2, 10 EGTA, 10 D-glucose, 10 HEPES, 5 MgATP, 0.4 Na3GTP, and 1 spermine, pH 7.2 (285–290 mOsm). Biocytin was added to the pipette for post hoc reconstruction to verify the identity of the cell as an interneuron, and not an ectopic CA1 pyramidal cell. Series resistance was monitored throughout each experiment with a −5-mV, 80-ms pulse before each stimulus, and cells with >20% change in series resistance were excluded from analysis. Data were digitized (5 kHz) and analyzed using macros written in IGOR-PRO (Wavemetrics, Lake Oswego, OR). To generate I-V curves, the holding potential was gradually increased to +40

mV, then 6 responses were recorded every 20 mV from +40 to −60 mV. Picrotoxin (100 μM) was added to block $GABA_A$R-mediated inhibition and d-APV (25 μM) was added to block NMDAR-mediated currents. Rectification index was defined as (amplitude of synaptic currents + 40 mV/amplitude of synaptic currents at −60 mV) multiplied by 1.5 to correct for differences in driving force; this correction assumes $E_{rev} = 0$. Representative I-V curves were corrected for a −8 mV junction potential.

For input-output, the stimulating voltage was increased from 10 to 50 V and EPSCs were recorded in the presence of picrotoxin (100 μM). The I/V curve was graphed by taking the average amplitude of 5 traces at each voltage stimulation. For anti-Hebbian LTP, cells were voltage-clamped at −60 mV in the presence of picrotoxin (100 μM). A stable baseline of 5 min or less was recorded at 0.1 Hz, due to reported wash-out of LTP. LTP was induced using a protocol pairing 400 pulses at 5 Hz, with postsynaptic hyperpolarization to −90 mV. All values are expressed as mean ± SEM. Statistical analysis was performed using Mann-Whitney test (Rectification Index), Two-sample *t*-test (Anti-Hebbian LTP), and the Two-way repeated measures ANOVA (Input-Output) using Origin Pro 2015 Software.

d-APV was purchased from Tocris. Salts for making ACSF, internal solutions, picrotoxin, and spermine were purchased from Sigma-Aldrich. All recordings and analyses were performed blind to genotype of the animal.

### QUANTIFICATION AND STATISTICAL ANALYSIS

Error bars of all data denote ± SEM. Differences between two groups were assessed by two tailed Student *t*-test and multiple groups were compared using one-way ANOVA for Figures 1, 2. 3, 4, 5, and 6. Statistical analysis of each data for Figure 7 is provided in Figure Legends. Differences were considered significant at $p < 0.05$; single, double, and triple asterisks indicate significant difference with $p < 0.05$, 0.01, or 0.001, respectively. The number of replicates for each experiment is indicated in the figure legends.

## Supplementary Material

Refer to Web version on PubMed Central for supplementary material.

## ACKNOWLEDGMENTS

We thank Fabrizio Pontarelli and Brenda Court-Vazquez for their technical assistance. This work was supported by NIH grants R01-MH092877 (to R.S.Z.), R01-MH125772, and R01-NS113600 (to P.E.C.); NARSAD Young Investigator Grant and LB692 Nebraska Biomedical Research Development Fund (to J.-Y.H.); NIH grant R21-NS118378 (to J.Y. and R.S.Z.); NARSAD Young Investigator Grant (to J.Y.); and NIH grant F31-MH114431 (to H.R.M.). R.S.Z. is the FM Kirby Professor in Neural Repair and Protection. The graphical abstract was created with BioRender.com.

## REFERENCES

Akgul G, and McBain CJ (2016). Diverse roles for ionotropic glutamate receptors on inhibitory interneurons in developing and adult brain. J. Physiol 594, 5471–5490. 10.1113/JP271764. [PubMed: 26918438]

Antoine MW, Langberg T, Schnepel P, and Feldman DE (2019). Increased excitation-inhibition ratio stabilizes synapse and circuit excitability in four autism mouse models. Neuron 101, 648–661.e4. 10.1016/j.neuron.2018.12.026. [PubMed: 30679017]

Ascano M Jr., Mukherjee N, Bandaru P, Miller JB, Nusbaum JD, Corcoran DL, Langlois C, Munschauer M, Dewell S, Hafner M, et al. (2012). FMRP targets distinct mRNA sequence elements to regulate protein expression. Nature 492, 382–386. 10.1038/nature11737. [PubMed: 23235829]

Bagni C, and Zukin RS (2019). A synaptic perspective of fragile X syndrome and autism spectrum disorders. Neuron 101, 1070–1088. 10.1016/j.neuron.2019.02.041. [PubMed: 30897358]

Batish M, van den Bogaard P, Kramer FR, and Tyagi S (2012). Neuronal mRNAs travel singly into dendrites. Proc. Natl. Acad. Sci. U S A 109, 4645–4650. 10.1073/pnas.1111226109. [PubMed: 22392993]

Bhakar AL, Dolen G, and Bear MF (2012). The pathophysiology of fragile X (and what it teaches us about synapses). Annu. Rev. Neurosci 35, 417–443. 10.1146/annurev-neuro-060909-153138. [PubMed: 22483044]

Bowie D, and Mayer ML (1995). Inward rectification of both AMPA and kainate subtype glutamate receptors generated by polyamine-mediated ion channel block. Neuron 15, 453–462. 10.1016/0896-6273(95)90049-7. [PubMed: 7646897]

Buxbaum AR, Wu B, and Singer RH (2014). Single beta-actin mRNA detection in neurons reveals a mechanism for regulating its translatability. Science 343, 419–422. 10.1126/science.1242939. [PubMed: 24458642]

Cajigas IJ, Tushev G, Will TJ, tom DS, Fuerst N, and Schuman EM (2012). The local transcriptome in the synaptic neuropil revealed by deep sequencing and high-resolution imaging. Neuron 74, 453–466. 10.1016/j.neuron.2012.02.036. [PubMed: 22578497]

Ceolin L, Bouquier N, Vitre-Boubaker J, Rialle S, Severac D, Valjent E, Perroy J, and Puighermanal E (2017). Cell type-specific mRNA dysregulation in hippocampal CA1 pyramidal neurons of the fragile X syndrome mouse model. Front. Mol. Neurosci 10, 340. 10.3389/fnmol.2017.00340. [PubMed: 29104533]

Darnell JC, and Klann E (2013). The translation of translational control by FMRP: therapeutic targets for FXS. Nat. Neurosci 16, 1530–1536. 10.1038/nn.3379. [PubMed: 23584741]

Darnell JC, Van Driesche SJ, Zhang C, Hung KY, Mele A, Fraser CE, Stone EF, Chen C, Fak JJ, Chi SW, et al. (2011). FMRP stalls ribosomal translocation on mRNAs linked to synaptic function and autism. Cell 146, 247–261. 10.1016/j.cell.2011.06.013. [PubMed: 21784246]

Das Sharma S, Metz JB, Li H, Hobson BD, Hornstein N, Sulzer D, Tang G, and Sims PA (2019). Widespread alterations in translation elongation in the brain of juvenile Fmr1 knockout mice. Cell Rep. 26, 3313–3322.e5. 10.1016/j.celrep.2019.02.086. [PubMed: 30893603]

Ding Q, Sethna F, Wu XT, Miao Z, Chen P, Zhang Y, Xiao H, Feng W, Feng Y, Li X, and Wang H (2020). Transcriptome signature analysis repurposes trifluoperazine for the treatment of fragile X syndrome in mouse model. Commun. Biol 3, 127. 10.1038/s42003-020-0833-4. [PubMed: 32179850]

Donnard E, Shu H, and Garber M (2020). Single cell transcriptomics reveals dysregulated cellular and molecular networks in a fragile X syndrome model. Preprint at bioRxiv. 10.1101/2020.02.12.946780.

Femino AM, Fay FS, Fogarty K, and Singer RH (1998). Visualization of single RNA transcripts in situ. Science 280, 585–590. 10.1126/science.280.5363.585. [PubMed: 9554849]

Fioriti L, Myers C, Huang YY, Li X, Stephan JS, Trifilieff P, Colnaghi L, Kosmidis S, Drisaldi B, Pavlopoulos E, and Kandel ER (2015). The persistence of hippocampal-based memory requires protein synthesis mediated by the prion-like protein CPEB3. Neuron 86, 1433–1448. 10.1016/j.neuron.2015.05.021. [PubMed: 26074003]

Ford L, Ling E, Kandel ER, and Fioriti L (2019). CPEB3 inhibits translation of mRNA targets by localizing them to P bodies. Proc. Natl. Acad. Sci. U S A 116, 18078–18087. 10.1073/pnas.1815275116. [PubMed: 31416913]

Fu YH, Kuhl DP, Pizzuti A, Pieretti M, Sutcliffe JS, Richards S, Verkert AJ, Holden JJ, Fenwick RG Jr., Warren ST, Oostra BA, Nelson DL, and Caskey C (1991). Variation of the CGG repeat at the fragile X site results in genetic instability: resolution of the Sherman paradox. Cell 67, 1047–1058. 10.1016/0092-8674(91)90283-5. [PubMed: 1760838]

Geiger JR, Melcher T, Koh DS, Sakmann B, Seeburg PH, Jonas P, and Monyer H (1995). Relative abundance of subunit mRNAs determines gating and Ca2+ permeability of

AMPA receptors in principal neurons and interneurons in rat CNS. Neuron 15, 193–204. 10.1016/0896-6273(95)90076-4. [PubMed: 7619522]

Grooms SY, Noh KM, Regis R, Bassell GJ, Bryan MK, Carroll RC, and Zukin RS (2006). Activity bidirectionally regulates AMPA receptor mRNA abundance in dendrites of hippocampal neurons. J. Neurosci 26, 8339–8351. 10.1523/jneurosci.0472-06.2006. [PubMed: 16899729]

Hagerman R, and Hagerman P (2013). Advances in clinical and molecular understanding of the FMR1 premutation and fragile X-associated tremor/ataxia syndrome. Lancet Neurol. 12, 786–798. 10.1016/s1474-4422(13)70125-x. [PubMed: 23867198]

Hagerman RJ, Berry-Kravis E, Hazlett HC, Bailey DB Jr., Moine H, Kooy RF, Tassone F, Gantois I, Sonenberg N, Mandel JL, and Hagerman PJ (2017). Fragile X syndrome. Nat. Rev. Dis. Primers 3, 17065. 10.1038/nrdp.2017.65. [PubMed: 28960184]

Ho VM, Dallalzadeh LO, Karathanasis N, Keles MF, Vangala S, Grogan T, Poirazi P, and Martin KC (2014). GluA2 mRNA distribution and regulation by miR-124 in hippocampal neurons. Mol. Cell Neurosci 61, 1–12. 10.1016/j.mcn.2014.04.006. [PubMed: 24784359]

Holt CE, and Schuman EM (2013). The central dogma decentralized: new perspectives on RNA function and local translation in neurons. Neuron 80, 648–657. 10.1016/j.neuron.2013.10.036. [PubMed: 24183017]

Huang YS, Kan MC, Lin CL, and Richter JD (2006). CPEB3 and CPEB4 in neurons: analysis of RNA-binding specificity and translational control of AMPA receptor GluR2 mRNA. EMBO J. 25, 4865–4876. 10.1038/sj.emboj.7601322. [PubMed: 17024188]

Hwang JY, Yan J, and Zukin RS (2019). Autophagy and synaptic plasticity: epigenetic regulation. Curr. Opin. Neurobiol 59, 207–212. 10.1016/j.conb.2019.09.010. [PubMed: 31634675]

Isaac JT, Ashby MC, and McBain CJ (2007). The role of the GluR2 subunit in AMPA receptor function and synaptic plasticity. Neuron 54, 859–871. 10.1016/j.neuron.2007.06.001. [PubMed: 17582328]

Ju W, Morishita W, Tsui J, Gaietta G, Deerinck TJ, Adams SR, Garner CC, Tsien RY, Ellisman MH, and Malenka RC (2004). Activity-dependent regulation of dendritic synthesis and trafficking of AMPA receptors. Nat. Neurosci 7, 244–253. 10.1038/nn1189. [PubMed: 14770185]

Kacharmina JE, Job C, Crino P, and Eberwine J (2000). Stimulation of glutamate receptor protein synthesis and membrane insertion within isolated neuronal dendrites. Proc. Natl. Acad. Sci. U S A 97, 11545–11550. 10.1073/pnas.97.21.11545. [PubMed: 11027353]

Kamboj SK, Swanson GT, and Cull-Candy SG(1995). Intracellular spermine confers rectification on rat calcium-permeable AMPA and kainate receptors. J. Physiol 486, 297–303. 10.1113/jphysiol.1995.sp020812. [PubMed: 7473197]

Korb E, Herre M, Zucker-Scharff I, Gresack J, Allis CD, and Darnell RB (2017). Excess translation of epigenetic regulators contributes to fragile X syndrome and is alleviated by Brd4 inhibition. Cell 170, 1209–1223.e20. 10.1016/j.cell.2017.07.033. [PubMed: 28823556]

Kullmann DM, and Lamsa K (2008). Roles of distinct glutamate receptors in induction of anti-Hebbian long-term potentiation. J. Physiol 586, 1481–1486. 10.1113/jphysiol.2007.148064. [PubMed: 18187472]

Kullmann DM, and Lamsa KP (2007). Long-term synaptic plasticity in hippocampal interneurons. Nat. Rev. Neurosci 8, 687–699. 10.1038/nrn2207. [PubMed: 17704811]

Lamsa KP, Heeroma JH, Somogyi P, Rusakov DA, and Kullmann DM (2007). Anti-Hebbian long-term potentiation in the hippocampal feedback inhibitory circuit. Science 315, 1262–1266. 10.1126/science.1137450. [PubMed: 17332410]

Larson DR, Singer RH, and Zenklusen D (2009). A single molecule view of gene expression. Trends Cell Biol 19, 630–637. 10.1016/j.tcb.2009.08.008. [PubMed: 19819144]

Le Roux N, Cabezas C, Bohm UL, and Poncer JC (2013). Input-specific learning rules at excitatory synapses onto hippocampal parvalbumin-expressing interneurons. J. Physiol 591, 1809–1822. 10.1113/jphysiol.2012.245852. [PubMed: 23339172]

Liu SJ, and Zukin RS (2007). Ca2+-permeable AMPA receptors in synaptic plasticity and neuronal death. Trends Neurosci. 30, 126–134. 10.1016/j.tins.2007.01.006. [PubMed: 17275103]

Liu Y, Wong TP, Aarts M, Rooyakkers A, Liu L, Lai TW, Wu DC, Lu J, Tymianski M, Craig AM, and Wang YT (2007). NMDA receptor subunits have differential roles in mediating

excitotoxic neuronal death both *in vitro* and *in vivo*. J. Neurosci 27, 2846–2857. 10.1523/jneurosci.0116-07.2007. [PubMed: 17360906]

Livak KJ, and Schmittgen TD (2001). Analysis of relative gene expression data using real-time quantitative PCR and the 2−ΔΔCT method. Methods 25, 402–408. 10.1006/meth.2001.1262. [PubMed: 11846609]

Lu W, Shi Y, Jackson AC, Bjorgan K, During MJ, Sprengel R, Seeburg PH, and Nicoll RA (2009). Subunit composition of synaptic AMPA receptors revealed by a single-cell genetic approach. Neuron 62, 254–268. 10.1016/j.neuron.2009.02.027. [PubMed: 19409270]

Mikl M, Vendra G, and Kiebler MA (2011). Independent localization of *MAP2*, *CaMKIIα* and *β-actin* RNAs in low copy numbers. EMBO Rep. 12, 1077–1084. 10.1038/embor.2011.149. [PubMed: 21869818]

Miyawaki T, Ofengeim D, Noh KM, Latuszek-Barrantes A, Hemmings BA, Follenzi A, and Zukin RS (2009). The endogenous inhibitor of Akt, CTMP, is critical to ischemia-induced neuronal death. Nat. Neurosci 12, 618–626. 10.1016/j.neures.2009.09.058. [PubMed: 19349976]

Mueller F, Senecal A, Tantale K, Marie-Nelly H, Ly N, Collin O, Basyuk E, Bertrand E, Darzacq X, and Zimmer C (2013). FISH-quant: automatic counting of transcripts in 3D FISH images. Nat. Methods 10, 277–278. 10.1038/nmeth.2406. [PubMed: 23538861]

Nelson SB, and Valakh V (2015). Excitatory/inhibitory balance and circuit homeostasis in autism spectrum disorders. Neuron 87, 684–698. 10.1016/j.neuron.2015.07.033. [PubMed: 26291155]

Nicholson E, and Kullmann DM (2014). Long-term potentiation in hippocampal oriens interneurons: postsynaptic induction, presynaptic expression and evaluation of candidate retrograde factors. Philos. Trans. R. Soc. Lond. B Biol. Sci 369, 20130133. 10.1098/rstb.2013.0133.

Noh KM, Hwang JY, Follenzi A, Athanasiadou R, Miyawaki T, Greally JM, Bennett MVL, and Zukin RS (2012). Repressor element-1 silencing transcription factor (REST)-dependent epigenetic remodeling is critical to ischemia-induced neuronal death. Proc. Natl. Acad. Sci. U S A 109, E962–E971. 10.1073/pnas.1121568109. [PubMed: 22371606]

Pavlopoulos E, Trifilieff P, Chevaleyre V, Fioriti L, Zairis S, Pagano A, Malleret G, and Kandel ER (2011). Neuralized1 activates CPEB3: a function for nonproteolytic ubiquitin in synaptic plasticity and memory storage. Cell 147, 1369–1383. 10.1016/j.cell.2011.09.056. [PubMed: 22153079]

Pieretti M, Zhang FP, Fu YH, Warren ST, Oostra BA, Caskey CT, and Nelson DL (1991). Absence of expression of the FMR-1 gene in fragile X syndrome. Cell 66, 817–822. 10.1016/0092-8674(91)90125-i. [PubMed: 1878973]

Racca C, Catania MV, Monyer H, and Sakmann B (1996). Expression of AMPA-glutamate receptor B subunit in rat hippocampal GABAergic neurons. Eur. J. Neurosci 8, 1580–1590. 10.1111/j.1460-9568.1996.tb01303.x. [PubMed: 8921250]

Raj A, van den Bogaard P, Rifkin SA, van Oudenaarden A, and Tyagi S (2008). Imaging individual mRNA molecules using multiple singly labeled probes. Nat. Methods 5, 877–879. 10.1038/nmeth.1253. [PubMed: 18806792]

Richter JD, Bassell GJ, and Klann E (2015). Dysregulation and restoration of translational homeostasis in fragile X syndrome. Nat. Rev. Neurosci 16, 595–605. 10.1038/nrn4001. [PubMed: 26350240]

Rodenas-Ruano A, Chavez AE, Cossio MJ, Castillo PE, and Zukin RS (2012). REST-dependent epigenetic remodeling promotes the developmental switch in synaptic NMDA receptors. Nat. Neurosci 15, 1382–1390. 10.1038/nn.3214. [PubMed: 22960932]

Ronesi JA, and Huber KM (2008). Metabotropic glutamate receptors and fragile x mental retardation protein: partners in translational regulation at the synapse. Sci. Signal 1, e6. 10.1126/stke.15pe6.

Savtchouk I, Sun L, Bender CL, Yang Q, Szabo G, Gasparini S, and Liu SJ (2016). Topological regulation of synaptic AMPA receptor expression by the RNA-binding protein CPEB3. Cell Rep. 17, 86–103. 10.1016/j.celrep.2016.08.094. [PubMed: 27681423]

Sawicka K, Hale CR, Park CY, Fak JJ, Gresack JE, Van Driesche SJ, Kang JJ, Darnell JC, and Darnell RB (2019). FMRP has a cell-type-specific role in CA1 pyramidal neurons to regulate autism-related transcripts and circadian memory. Elife 8, e46919. 10.7554/elife.46919. [PubMed: 31860442]

Szabo A, Somogyi J, Cauli B, Lambolez B, Somogyi P, and Lamsa KP (2012). Calcium-permeable AMPA receptors provide a common mechanism for LTP in glutamatergic synapses of distinct

hippocampal interneuron types. J. Neurosci 32, 6511–6516. 10.1523/jneurosci.0206-12.2012. [PubMed: 22573673]

Wang DO, Martin KC, and Zukin RS (2010). Spatially restricting gene expression by local translation at synapses. Trends Neurosci. 33, 173–182. 10.1016/j.tins.2010.01.005. [PubMed: 20303187]

Yan J, Porch MW, Court-Vazquez B, Bennett MVL, and Zukin RS (2018). Activation of autophagy rescues synaptic and cognitive deficits in fragile X mice. Proc. Natl. Acad. Sci. U S A 115, E9707–E9716. 10.1073/pnas.1808247115. [PubMed: 30242133]

Zenklusen D, Larson DR, and Singer RH (2008). Single-RNA counting reveals alternative modes of gene expression in yeast. Nat. Struct. Mol. Biol 15, 1263–1271. 10.1038/nsmb.1514. [PubMed: 19011635]

## Highlights

- Transcription of GluA2 mRNA is elevated in *Fmr1*-deficient hippocampal neurons
- CPEB3 and STAT5b are the upstream effectors critical to GluA2 mRNA expression
- Increase in GluA2 underlies a switch in synaptic AMPAR phenotype in CA1 interneurons
- A switch in AMPAR phenotype causes deficits in synaptic transmission and plasticity

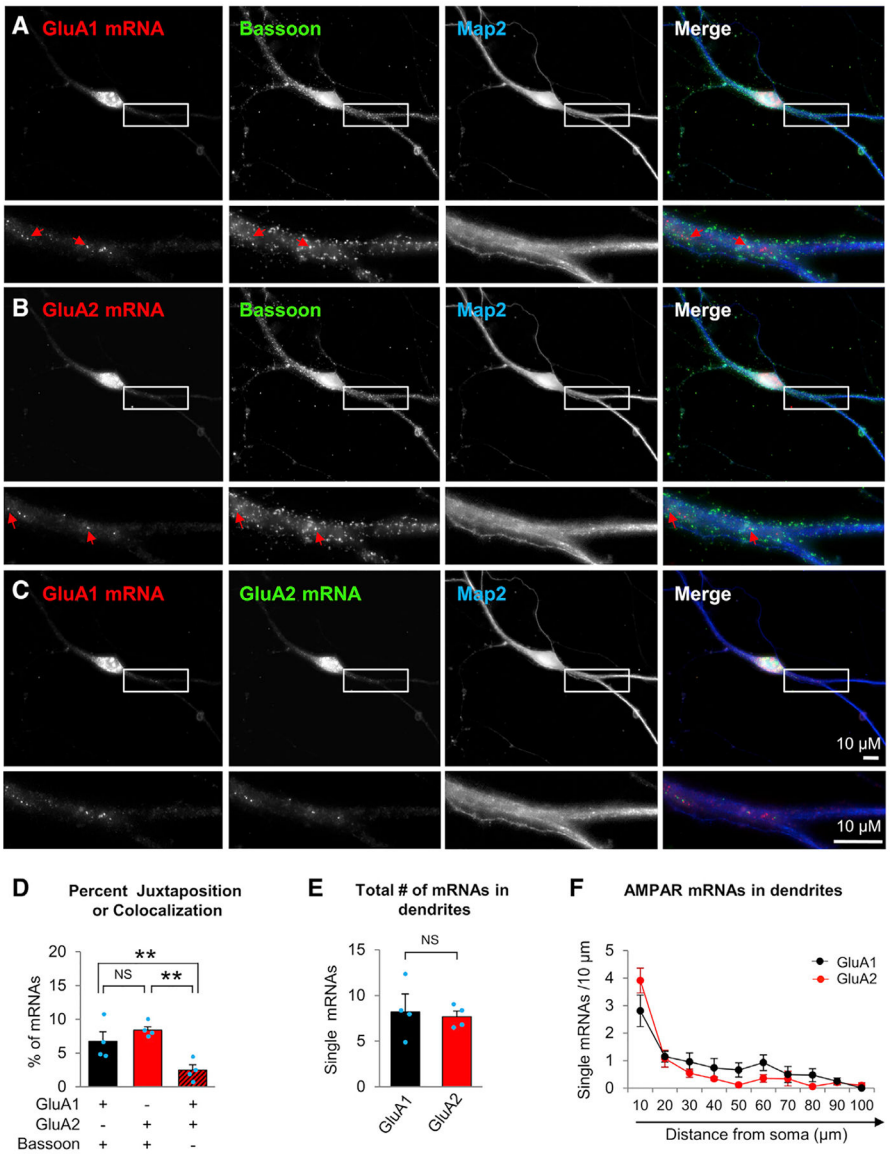


**Figure 1. mRNAs encoding AMPAR subunits localize to proximal dendrites and synaptic sites in WT neurons**

(A and B) Upper: representative images of individual endogenous GluA1 (red) (A) or GluA2 (red) (B) mRNA molecules within a single hippocampal neuron detected by single-molecule FISH, followed by immunofluorescence with antibodies directed to the presynaptic marker bassoon (green), the dendritic marker MAP2 (blue), and merge. Lower: higher-magnification images of boxed region in the upper panel.

(C) Upper: representative images of individual GluA1 (red) and GluA2 (green) mRNA molecules in the same neuron. Lower: higher-magnification images.

(D) Summary data of images like those in (A and B) showing the number of AMPAR GluA1 (black) and GluA2 (red) mRNAs that juxtapose to synaptic sites marked by basoon (first two bars) or that colocalize with each other (third bar). GluA1 and GluA2, 30dendrites, 30 neurons, n = 4.

(E) Summary data for images like those in (C) showing the number of GluA1 and GluA2 molecules per dendrite.
(F) GluA1 and GluA2 mRNA molecules as a function of the distance from the soma (GluA1, 101 dendrites, 35 neurons, n = 4; GluA2, 190 dendrites, 82 neurons, n = 4).
The number of individual GluA1 and GluA2 mRNA molecules in all dendrites of all hippocampal neurons that met the criteria for identification as mRNAs (STAR Methods) were analyzed by an individual blinded to the treatment. Scale bar, 10 μm. For (D–F): Data are mean ± SEM. **p < 0.01. NS, not significant. Here and in Figures 2, 3, 4 (with the exception of Figure 2L), S1, and S2, n is defined as number of independent experiments each involving a different batch of neurons. In Figure 2I, n is defined as number of animals.

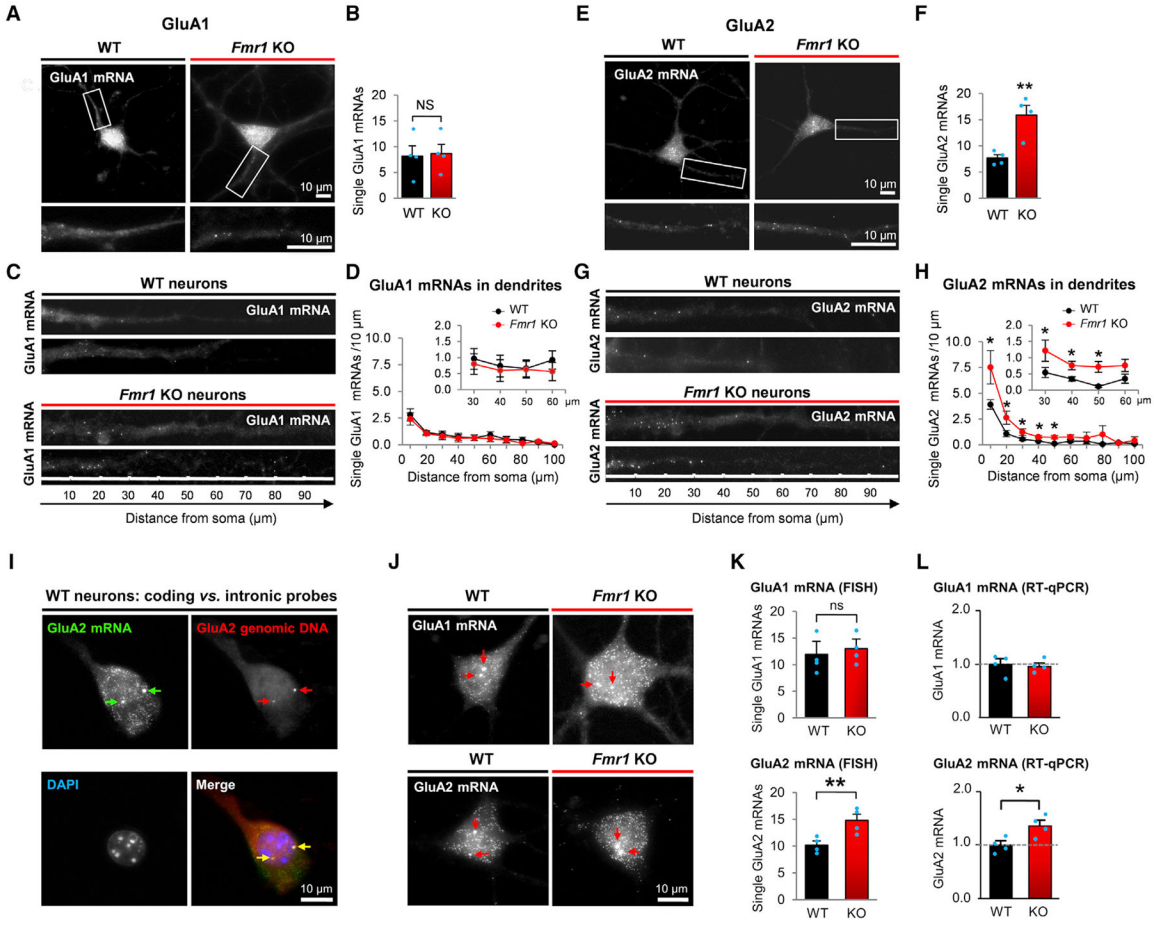


**Figure 2. GluA2 (but not GluA1) mRNA is elevated in dendrites and at TSSs of hippocampal neurons from *Fmr1* KO mice**

(A–D) Representative images of endogenous single mRNAs molecules encoding GluA1 were detected by single-molecule FISH in primary cultures of hippocampal neurons from WT and *Fmr1* KO mice (A) quantified in (B). (C) Higher-magnification images of boxed region in (A) quantified in (D).

(E–H) Representative images of endogenous single mRNAs molecules encoding GluA2 were detected by single-molecule FISH in primary cultures of hippocampal neurons from WT and *Fmr1* KO mice (E) quantified in (F). (G) Higher-magnification images of boxed region in (E) quantified in (H) (GluA1, WT: 101 dendrites, 35 neurons; KO: 134 dendrites, 63 neurons, n = 4 per group; GluA2, WT: 190 dendrites, 82 neurons; KO: 99 dendrites, 82 neurons, n = 4 per group).

(I) Representative images of a dual FISH experiment with probes targeting either the GluA2 coding (upper left) or intronic (upper right) sequences.

(J) Representative images showing the number of GluA1 and GluA2 mRNA molecules at transcription hotspots in the nucleus of neurons from WT and *Fmr1* KO mice.

(K) Summary data of images like those illustrated in (J) (GluA1, WT: 35 neurons; KO: 63 neurons; GluA2, WT: 82 neurons, KO: 86 neurons, n = 4).

(L) Summary qRT-PCR data from whole hippocampus showing GluA1 (upper) and GluA2 (lower) mRNA expression (n = 4 per group). For all the quantitative graphs: Data are mean ± SEM. *p < 0.05; **p < 0.01.

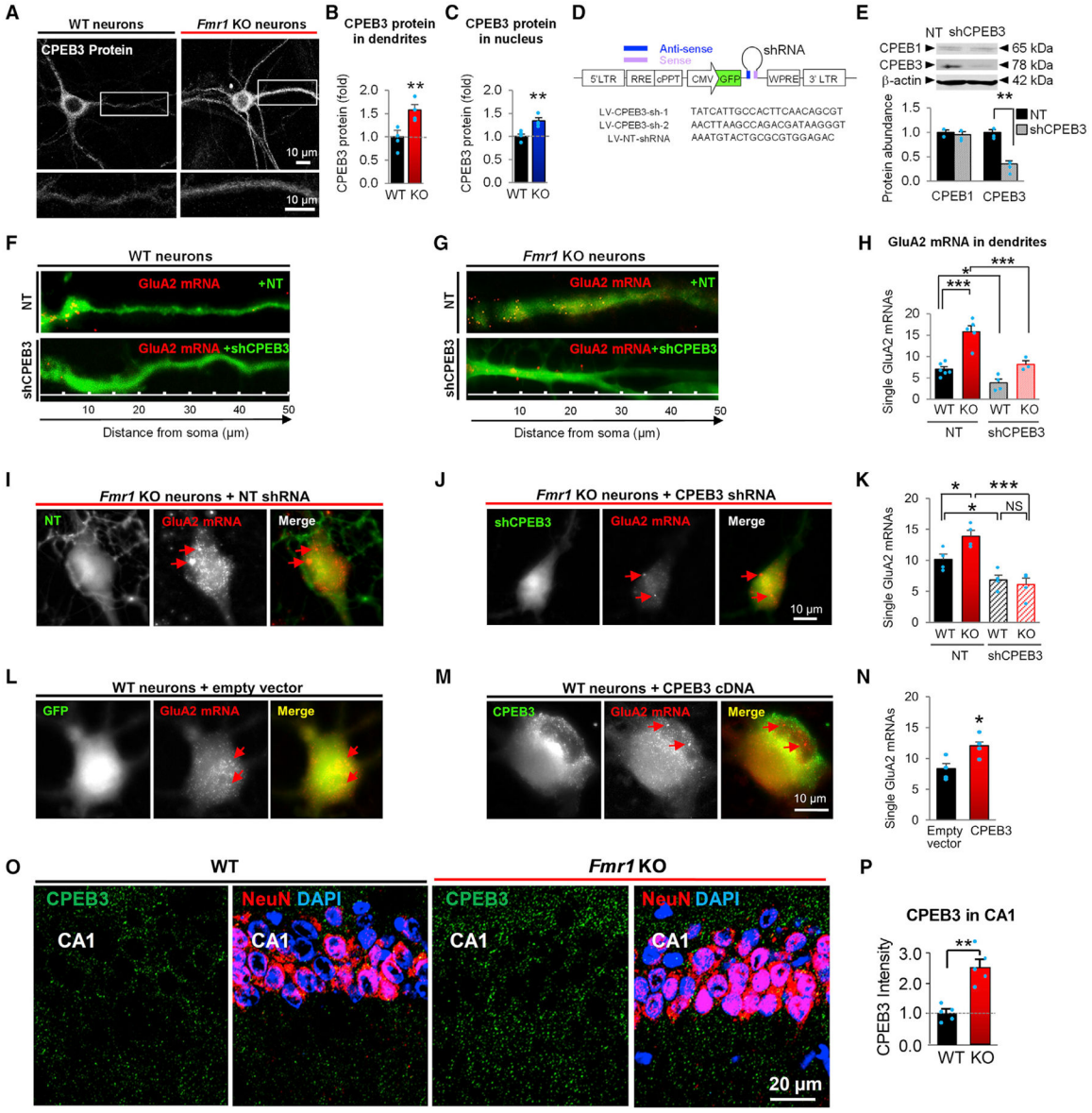


**Figure 3. CPEB3 protein is elevated in dendrites and at TSSs of hippocampal neurons from *Fmr1* KO mice and is critical to elevated GluA2 mRNA**

(A) Upper: representative immunofluorescence images of WT and *Fmr1* KO hippocampal neurons at low magnification. Lower: high-resolution image of boxed dendrite illustrated in the upper panel.

(B and C) Summary data for images like those in (A) showing relative dendritic (B) and nuclear (C) abundance of CPEB3 protein (WT: 35 dendrites, 19 neurons; KO: 28 dendrites, 21 neurons, n = 4 per group).

(D) Schematic representation of the lentivirus construct containing CPEB3 shRNA-1, shRNA-2, and NT shRNA.

(E) Representative western blot showing efficacy and specificity of CPEB3 shRNA-1 (n = 3).

(F and G) Images of a merge between GluA2 mRNA, assessed by FISH (red) and GFP, assessed by immunofluorescence (green) in dendrites taken from the first 50 μm of dendrites, as measured from the cell body of hippocampal neurons from WT (F) and *Fmr1* KO mice (G). Upper, NT shRNA; lower, CPEB3 shRNA-1.

(H) Summary data for images like those illustrated in (F and G) (WT + NT shRNA, 57 dendrites; KO + NT shRNA: 59 dendrites; WT + CPEB3 shRNA: 31 dendrites; KO + CPEB3 shRNA: 33 dendrites, n = 3–6 per group).

(I and J) Representative images of *Fmr1* KO neurons expressing NT (I) or CPEB3 (J) shRNA and labeled for GluA2 mRNA.

(K) Summary data of images like those in (I and J) (WT + NT: 139 neurons; *Fmr1* KO + NT shRNA: 163 neurons; WT + CPEB3 shRNA: 52 neurons; *Fmr1* KO + CPEB3 shRNA: 50 neurons, n = 4 per group).

(L and M) Representative images of WT neurons expressing (L) GFP or (M) GFP-tagged CPEB3 and labeled for GluA2 mRNA.

(N) Summary data of images like those in (L and M) (empty vector: 85 neurons; CPEB3 cDNA: 102 neurons, n = 4 per group).

(O) CPEB3 immunofluorescence in neurons marked by NeuN of the CA1 in brain sections from WT and *Fmr1* KO mice.

(P) Quantification of immunofluorescence puncta in images like that illustrated in (O) (n = 5 mice per group). For all the quantitative graphs: Data are mean ± SEM. *p < 0.05; **p < 0.01; ***p < 0.001.

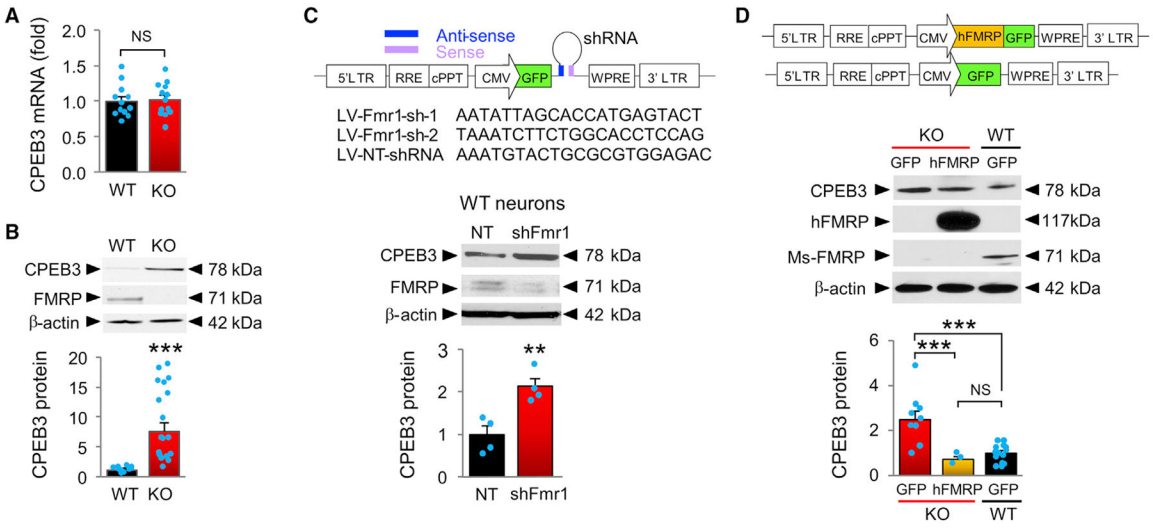


**Figure 4. Loss of FMRP is causally related to the elevated CPEB3 in fragile X neurons**

(A) Summary data showing CPEB3 mRNA expression in hippocampal neurons from *Fmr1* KO versus WT mice (n = 12–13/coverslips).

(B) Representative western blot (upper) and summary data (lower) showing CPEB3 protein abundance in neurons from *Fmr1* KO versus WT neurons (n = 9–18 coverslips).

(C) Upper: schematic of shRNA constructs. Lower: representative western blot of WT neurons expressing *Fmr1* shRNA or NT shRNA (negative control) and summary data showing FMRP and CPEB3 protein abundance.

(D) Upper: schematic of human FMRP cDNA and empty vector. Lower: representative western of WT and *Fmr1* KO neurons expressing either empty vector (GFP) or hFMRP-GFP and summary data showing human (h) and mouse (Ms) FMRP, and CPEB3 abundance in WT and *Fmr1* KO neurons (n = 3–12 wells/coverslips, 3 independent experiments). For all the quantitative graphs: Data are mean ± SEM. **p < 0.01; ***p < 0.001.

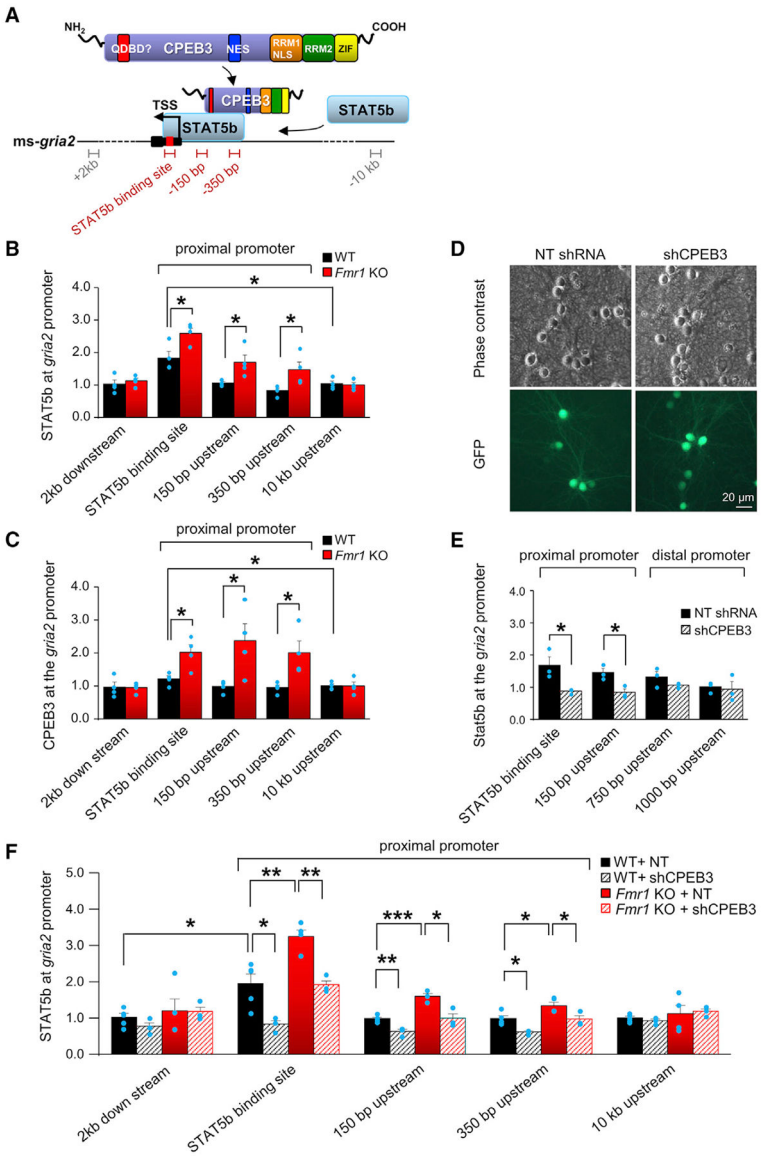


**Figure 5. CPEB3 binds the *gria2* promoter and enhances Stat5b-dependent GluA2 transcription**

(A) Schematic of the *gria2* promoter region highlighting the putative STAT5b binding motif and sites proximal and distal to the TSS to which probes were designed. Also shown are models of CPEB3 depicting a nuclear export sequence, a nuclear localization sequence, two RNA binding domains, and a gluta-mine-rich binding domain within the N terminus, which serves as a binding site for STAT5b and STAT5b, depicting a zinc-finger-binding domain harbored within the C terminus which enables binding to DNA.

(B) ChIP-qPCR showing enrichment of the transcription factor STAT5b at the proximal *gria2* promoter in the hippocampus of WT and *Fmr1* KO mice (n = 4 mice per group). The fold change for each group was normalized to the value obtained at a site 10 kb upstream of the TSS in WT.

(C) ChIP-qPCR showing enrichment of CPEB3 at the putative STAT5b binding motif within the *gria2* promoter in WT and *Fmr1* KO mice (n = 4 mice per group; the fold change of each group was normalized to the value 10 kb upstream in WT).
(D) Representative GFP fluorescence images showing expression of CPEB3 shRNA and NT shRNA in primary cultures of hippocampal neurons.
(E) ChIP-qPCR showing enrichment of STAT5b at the putative STAT5b recognition motif and sites proximal (150 bp upstream) and distal (750 or 1,000 bp upstream) from the TSS within the *gria2* promoter in CPEB3 or NT shRNA-treated primary cultures of hippocampal neurons (n = 3 experiments; the fold change for each group was normalized to the value for STAT5b occupancy 1 kb upstream of the TSS in *gria2* in NT shRNA-treated neurons).
(F) ChIP-qPCR showing enrichment of STAT5b at the putative STAT5b recognition motif and sites proximal (150 and 350 bp upstream) and distal (2 kb downstream or 10 kb upstream) from the TSS within the *gria2* promoter in the hippocampus of WT and *Fmr1 KO* mice *in vivo* (n = 3–5 mice per group; the fold change for each group is normalized to the value for STAT5b binding to a site 10 kb upstream in the hippocampus of NT shRNA-treated WT mice). For all the quantitative graphs: Data are mean ± SEM. *$p < 0.05$; **$p < 0.01$; ***$p < 0.001$.

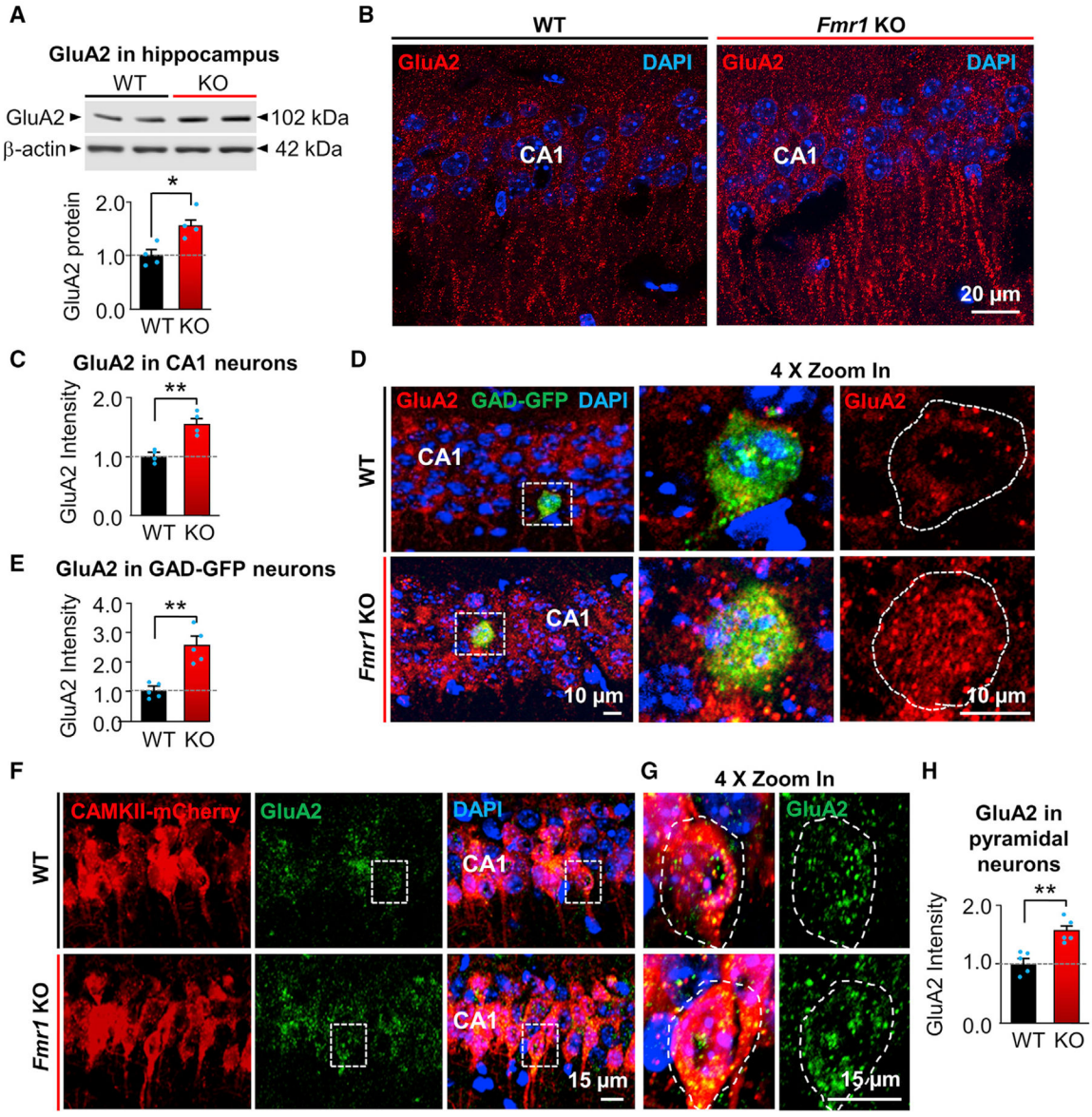


**Figure 6. CA1 inhibitory interneurons of *Fmr1* KO mice express elevated GluA2 protein and exhibit properties of GluA2-containing AMPARs**

(A) Representative western blot (upper) and summary data (lower) showing GluA2 protein abundance in the hippocampus of WT and *Fmr1 KO* mice at P21.

(B) Representative images of GluA2 immunofluorescence showing GluA2 protein expression in the cell bodies and dendrites of pyramidal neurons in the hippocampal CA1 from WT and *Fmr1* KO mice at P21.

(C) Summary of data from images like those illustrated in (B) (WT: 12 sections, 4 mice; *Fmr1* KO: 12 sections, 4 mice). Sections were selected as one from every six serial sections.

(D) Left: Representative immunofluorescence images of GluA2 protein expression in the *stratum pyramidale* of WT (upper) and *Fmr1* KO (lower) mice expressing GAD67-GFP at P21. Center: high-magnification (43 zoomed) images of boxed area on left shows a

GAD67(+) neuron. Right: GluA2 expression in the GAD67-GFP(+) neuron illustrated in center.

(E) Summary data for GluA2 protein expression in GAD67-GFP(+) neurons like that illustrated in (D) (WT: 15 cells, 5 mice; *Fmr1* KO: 15 cells, 5 mice).

(F) WT and *Fmr1* KO mice were injected with AAV-CAMKII-mCherry directly into CA1 to label pyramidal neurons. Representative images of mCherry fluorescence (left), GluA2 immunofluorescence (center), and DAPI label (merge, right) in the CA1 *stratum pyramidale* of WT (upper) and *Fmr1* KO (lower) mice at P21.

(G) High-magnification (4× zoomed) image of the boxed area in (F) shows mCherry(+) pyramidal neurons (left) expressing GluA2 protein (right).

(H) Summary data from images like that illustrated in (G) (WT: 20 cells, 5 mice; *Fmr1* KO: 20 cells, 5 mice). For all the quantitative graphs: Data are mean ± SEM. *$p < 0.05$; **$p < 0.01$.

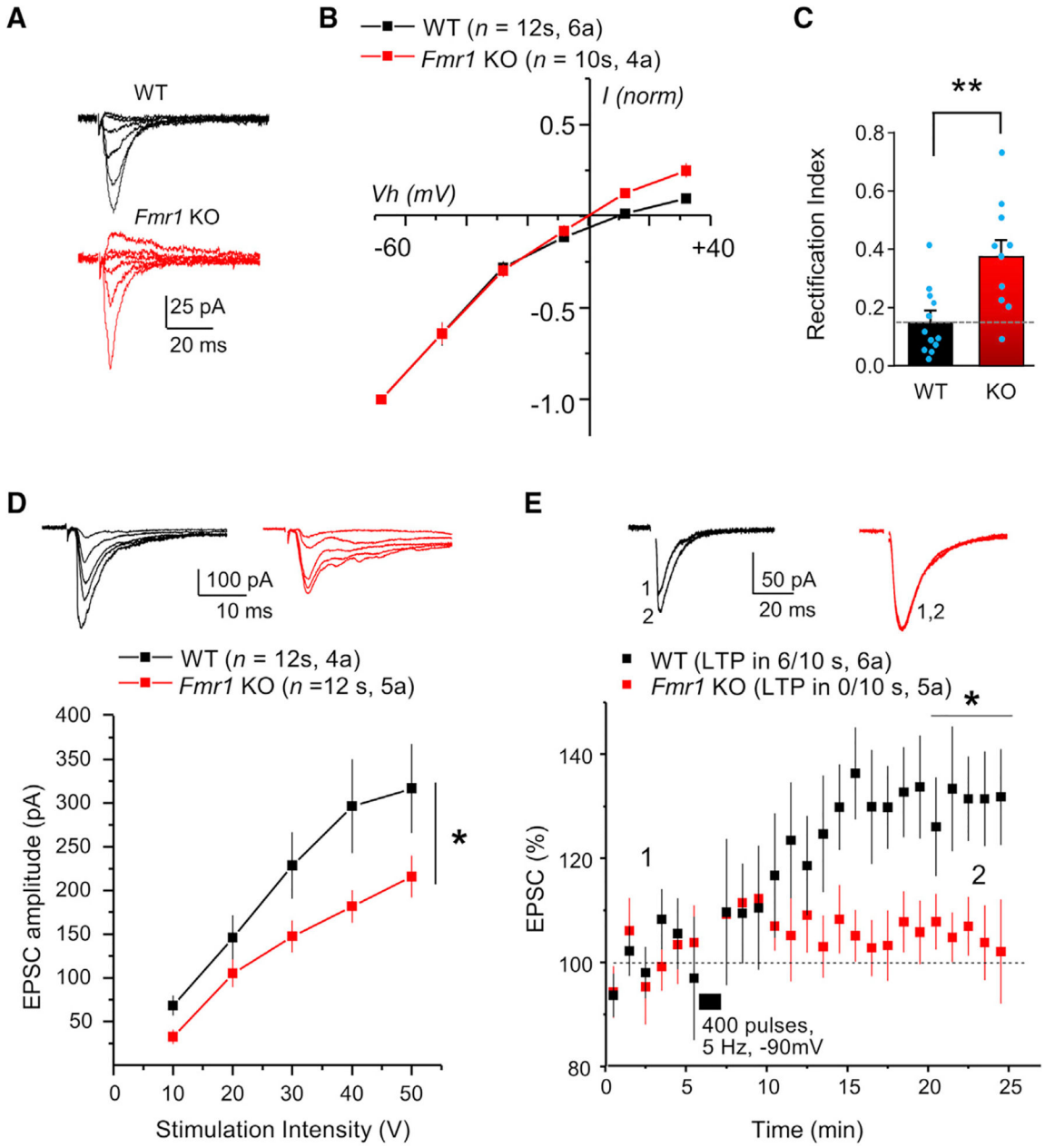


**Figure 7. Inhibitory interneurons in the CA1 of *Fmr1* KO mice exhibit deficits in synaptic transmission and plasticity**

(A) Representative AMPAR-EPSCs recorded from CA1 interneurons in acute hippocampal slices from mice at P14-P21 in the presence of 25 μM d-APV and 100 μM picrotoxin (bath) and 1 mM spermine (pipette).

(B) The normalized average I-V relationship of AMPAR-EPSC peak amplitudes showed characteristic inward rectification in slices from WT mice. AMPAR-EPSC peak amplitudes recorded from *Fmr1* KO mice exhibited linearization of the I-V relationship at positive potentials (WT: 12 cells, 6 mice; *Fmr1* KO: 10 cells, 4 mice).

(C) The rectification index (EPSC amplitude at 40 mV/EPSC amplitude at −60 mV) × 1.5) in WT and *Fmr1* KO mice. Mann-Whitney test, p = 0.0051.

(D) Upper: representative EPSCs recorded from CA1 interneurons in acute hippocampal slices from P14-P25 mice. Lower: average input-output relationship of EPSC peak amplitudes at five stimulation intensities in WT and *Fmr1* KO mice (WT: 10 cells, 4 mice; *Fmr1* KO: 10 cells, 5 mice), two-way ANOVA, $p = 0.003$, $F = 11.78$.
(E) NMDAR-independent LTP at glutamatergic synapses onto inhibitory GABAergic interneurons observed in slices from WT and *Fmr1* KO mice. CA1 interneurons were identified and voltage clamped at 60 mV using the visualized patch technique (WT: 10 cells, 4 mice; *Fmr1* KO: 10 cells, 5 mice); mean ± SEM of WT: 128.900 ± 8.712 versus *Fmr1* KO: 104.403 ± 4.339, two-sample t test, $p = 0.022$.

## KEY RESOURCES TABLE

| REAGENT or RESOURCE | SOURCE | IDENTIFIER |
|---|---|---|
| Antibodies | | |
| Rabbit polyclonal anti-CPEB3 | Abcam | Cat# ab10883; RRID:AB_442831 |
| Rabbit polyclonal anti-CPEB1 | Abcam | Cat# ab3465; RRID:AB_303826 |
| Rabbit polyclonal anti-FMRP | Abcam | Cat# ab27455; RRID:AB_732400 |
| Mouse monoclonal anti-GluR2 (GluA2) | BD Biosciences | Cat# 556341; RRID:AB_396373 |
| Mouse monoclonal anti- β-Actin | Sigma | Cat# A5316; RRID:AB_476743 |
| Mouse monoclonal anti-Bassoon | Enzo Life Sciences | Cat# ADI-VAM-PS003; RRID:AB_10618753 |
| Mouse monoclonal anti-Stat5b | Santa Cruz Biotechnology | Cat# sc-1656; RRID:AB_2197067 |
| Rabbit polyclonal anti-Synapsin I | Abcam | Cat# ab64581; RRID:AB_1281135 |
| Rabbit polyclonal anti-AMPA Receptor 1 (GluR1)/GluA1 | Alomone Labs | Cat# AGC-004; RRID:AB_2039878 |
| Rabbit polyclonal anti-VGLUT1 | Thermo Fisher Scientific | Cat# 48–2400; RRID:AB_2533843 |
| Mouse monoclonal anti-GAD67 | Millipore | Cat# MAB5406; RRID:AB_2278725 |
| Mouse monoclonal anti-NeuN | Millipore | Cat# MAB337; RRID:AB_2313673 |
| Chicken polyclonal anti-MAP2 | Millipore | Cat# AB15452; RRID:AB_805385 |
| Anti-mouse IgG, HRP-linked antibody | Cell Signaling Technology | Cat# 7076; RRID:AB_330924 |
| Anti-Rabbit IgG, HRP-linked antibody | Cell Signaling Technology | Cat# 7074; RRID:AB_2099233 |
| DyLight™ 405 AffiniPure Donkey Anti-Chicken IgY (IgG) (H+L) | Jackson ImmunoResearch Labs | Cat# 703-475-155; RRID:AB_2340373 |
| Alexa Fluor 488 Polyclonal Antibody | Invitrogen | Cat# A-11094; RRID:AB_221544 |
| Goat anti-Rabbit IgG (H+L) Cross-Adsorbed Secondary Antibody, Alexa Fluor™ 546 | Invitrogen | Cat# A-11010, RRID:AB_2534077) |
| Goat anti-Mouse IgG, IgM (H+L) Secondary Antibody, Alexa Fluor™ 488 | Invitrogen | Cat# A-10680; RRID:AB_2534062 |
| Goat anti-Mouse IgG (H+L) Cross-Adsorbed Secondary Antibody, Alexa Fluor™ 546 | Invitrogen | Cat# A-11030; RRID:AB_2534089 |
| Donkey anti-Rabbit IgG (H+L) Highly Cross-Adsorbed Secondary Antibody, Alexa Fluor™ 647 | Invitrogen | Cat# A-31573; RRID:AB_2536183 |
| Bacterial and virus strains | | |
| AAV-CaMKIIa-mCherry | Addgene | #114469 |
| LV-eGFP-tagged rCPEB3 | This paper | N/A |
| LV-eGFP-tagged hFMRP | This paper | N/A |
| LV-Fmr1 shRNA1 | This paper | N/A |
| LV-Fmr1 shRNA2 | This paper | N/A |
| LV-non-targeting shRNA | Noh et al., 2012 | N/A |
| LV-CPEB3 shRNA1 | This paper | N/A |
| LV-CPEB3 shRNA2 | This paper | N/A |
| Chemicals, peptides, and recombinant proteins | | |
| NBQX | Tocris | Cat#0373/10, CAS: 118876-58-7 |
| d-APV | Tocris | Cat#0106, CAS: 79055-68-8 |

| REAGENT or RESOURCE | SOURCE | IDENTIFIER |
|---|---|---|
| Picrotoxin | Sigma | Cat#P1675, CAS: 124-87-8 |
| Spermine | Sigma | Cat# S4264, CAS: 71-44-3 |
| Experimental models: Cell lines | | |
| HEK293T | ATCC | Cat# CRL-3216 |
| Experimental models: Organisms/strains | | |
| Mouse: FVB.129P2-Pde6b+ Tyrc-ch *Fmr1* tm1Cgr/J female | The Jackson Laboratory | RRID:IMSR_JAX:004624 |
| Mouse: FVB.129P2-Pde6b+ Tyrc-ch/AntJ male | The Jackson Laboratory | RRID:IMSR_JAX:004828 |
| Mouse: CB6-Tg(Gad1-EGFP) G42Zjh/J | The Jackson Laboratory | RRID:IMSR_JAX:007677 |
| Oligonucleotides | | |
| siRNA targeting sequence: CPEB3 shRNA-1: 5′-AACTTAAGCCAGACGATAAGGGT-3′ | This paper | N/A |
| siRNA targeting sequence: CPEB3 shRNA-2: 5′-TAAATGTACTGCGCGTGGA GAC-3′ | This paper | N/A |
| siRNA targeting sequence: Fmr1 shRNA-1: 5′-AATATTAGCACCATGAGTACC-3′ | This paper | N/A |
| siRNA targeting sequence: Fmr1 shRNA-2: 5′-TAAATCTTCTGGCACCTCCAG-3′ | This paper | N/A |
| Non-targeting shRNA sequence: NT shRNA: 5′-AAATGTACTGCG CGT GGAGAC-3′ | This paper | N/A |
| FISH probes for GluA1 anti-sense, GluA2 anti-sense and GluA2 intronic antisense, see Table S1 | This paper | N/A |
| ChIP primers for rat gria2 stat5b binding site:<br>Forward CAAGAAAAGTAGAGCATCCACAAAAT<br>Reverse AAACAGTCAAAGAAGGAAGAGGAAGA | This paper | N/A |
| ChIP primers for rat gria2 ~150 bp upstream from the TSS:<br>Forward CAGTCTTGCGCATCCGATT<br>Reverse AGCCCAGAGCTCCGACTAAAG | This paper | N/A |
| ChIP primers for rat gria2 ~750 bp from the TSS:<br>Forward TGGATTGAAAGGAACCGTAGGT<br>Reverse CAGATTATGGACATCCTTTCTAGACAAC | This paper | N/A |
| ChIP primers for rat gria2 ~1000 bp from the TSS:<br>Forward GCTTGGTGAAGACTCCTGATGATT<br>Reverse GCTTGGCATGAAGTAGAATATTGAAC | This paper | N/A |
| ChIP primers for mouse gria2 stat5b binding site:<br>Forward CCAAGAAAAGTAGAGCATCCACAA<br>Reverse AAACGGTCAAAGAAGGAAAAGGA | This paper | N/A |
| ChIP primers for mouse gria2 ~150 bp upstream from the TSS:<br>Forward GGCAGCCTGGTGCCTCTTA<br>Reverse TCCGCGGTGCTAAAATCG | This paper | N/A |
| ChIP primers for mouse gria2 ~350 bp upstream from the TSS:<br>Forward GGCGGCGAAGCTTTCTTC<br>Reverse TCAAATCATATTCGTTGTGCTCAA | This paper | N/A |
| ChIP primers for mouse gria2 ~2 kb downstream from the TSS:<br>Forward CGGGCCCAACTCCTCAA<br>Reverse AGCCCCACGTCGTCCTATT | This paper | N/A |
| ChIP primers for mouse gria2 ~10 kb upstream from the TSS:<br>Forward CAGACAACAGCAACACGGAATAG<br>Reverse CCTACAGCTTTGACCAGCTTCTC | This paper | N/A |
| Recombinant DNA | | |
| Plasmid: FCGW-GFP-hFMRP | This paper | N/A |
| Plasmid: FCGW-GFP-rCPEB3 | This paper | N/A |
| Software and algorithms | | |

| REAGENT or RESOURCE | SOURCE | IDENTIFIER |
|---|---|---|
| ImageJ | | https://imagej.nih.gov/ij/ |